

Receptor Activity-modifying Proteins 2 and 3 Generate Adrenomedullin Receptor Subtypes with Distinct Molecular Properties^{*[S]}

Received for publication, September 3, 2015, and in revised form, March 20, 2016. Published, JBC Papers in Press, March 24, 2016, DOI 10.1074/jbc.M115.688218

Harriet A. Watkins^{‡§1}, Madhuri Chakravarthy[‡], Rekhati S. Abhayawardana[‡], Joseph J. Gingell^{‡§}, Michael Garelja[‡], Meenakshi Pardamwar[¶], James M. W. R. McElhinney[¶], Alex Lathbridge[¶], Arran Constantine[¶], Paul W. R. Harris^{§||}, Tsz-Ying Yuen^{§||}, Margaret A. Brimble^{§||}, James Barwell^{§||}, David R. Poyner^{**}, Michael J. Woolley^{‡‡3}, Alex C. Conner^{‡‡}, Augen A. Pioszak^{§§}, Christopher A. Reynolds^{¶4}, and  Debbie L. Hay^{‡§1,5}

From the [‡]School of Biological Sciences, the [§]Maurice Wilkins Centre for Molecular Biodiscovery, and the ^{||}School of Chemical Sciences, University of Auckland, Auckland 1010, New Zealand, the [¶]School of Biological Sciences, University of Essex, Wivenhoe Park, Colchester CO4 3SQ, United Kingdom, the ^{**}School of Life and Health Sciences, Aston University, Aston Triangle, Birmingham B4 7ET, United Kingdom, the ^{‡‡}School of Clinical and Experimental Medicine, University of Birmingham, Edgbaston, Birmingham B15 2TT, United Kingdom, the ^{§§}Department of Biochemistry and Molecular Biology, University of Oklahoma Health Sciences Center, Oklahoma City, Oklahoma 73104

Adrenomedullin (AM) is a peptide hormone with numerous effects in the vascular systems. AM signals through the AM₁ and AM₂ receptors formed by the obligate heterodimerization of a G protein-coupled receptor, the calcitonin receptor-like receptor (CLR), and receptor activity-modifying proteins 2 and 3 (RAMP2 and RAMP3), respectively. These different CLR-RAMP interactions yield discrete receptor pharmacology and physiological effects. The effective design of therapeutics that target the individual AM receptors is dependent on understanding the molecular details of the effects of RAMPs on CLR. To understand the role of RAMP2 and -3 on the activation and conformation of the CLR subunit of AM receptors, we mutated 68 individual amino acids in the juxtamembrane region of CLR, a key region for activation of AM receptors, and determined the effects on cAMP signaling. Sixteen CLR mutations had differential effects between the AM₁ and AM₂ receptors. Accompanying this, independent molecular modeling of the full-length AM-bound AM₁ and AM₂ receptors predicted differences in the binding pocket and differences in the electrostatic potential of the two AM receptors. Druggability analysis indicated unique features that could be used to develop selective small molecule ligands for each receptor. The interaction of RAMP2 or RAMP3 with CLR induces conformational variation in the juxtamembrane region, yielding distinct binding pockets, probably via an

allosteric mechanism. These subtype-specific differences have implications for the design of therapeutics aimed at specific AM receptors and for understanding the mechanisms by which accessory proteins affect G protein-coupled receptor function.

The endothelium-derived peptide hormone adrenomedullin (AM)⁶ is a protective factor in the cardiovascular system and a biomarker for cardiovascular disease (1–5). AM administration in human subjects has several positive outcomes, significantly improving patient recovery from myocardial infarction, inhibiting myocyte apoptosis, reducing mean pulmonary arterial pressure, and increasing cardiac output in heart failure patients (1, 5–7). However, serious adverse hypotension in some patients, coupled with rapid metabolism of the peptide, means that optimal targeting of the AM system still needs to be achieved (7, 8). The pro-angiogenic effects of AM mean that receptor agonists or antagonists could be useful in a range of other conditions, such as lymphedema or cancer (9). Realizing any of these therapeutic goals, however, requires a much greater understanding of AM receptor biology. Here we explore receptor architecture to lay the foundations for the design of selective AM receptor ligands.

AM signals through two receptors. These both contain the calcitonin receptor-like receptor (CLR), a class B G protein-coupled receptor (GPCR) that has an absolute requirement for association with a receptor activity-modifying protein (RAMP) for ligand binding and receptor activation to occur. Association of CLR with RAMP2 generates the AM₁ receptor, whereas CLR with RAMP3 forms the AM₂ receptor (10).

The AM₁ receptor has an important role in cardiovascular system development. Deletion of the genes for AM, CLR, or

^{*} This work was supported in part by Biotechnology and Biological Sciences Research Council Grants BB/M006883/1 (to C. A. R.) and BB/M007529/1 and BB/M000176/1 (to D. P.). The authors declare that they have no conflicts of interest with the contents of this article.

✂ Author's Choice—Final version free via Creative Commons CC-BY license.

[S] This article contains supplemental PDB models 1 and 2.

¹ Supported by the National Heart Foundation of New Zealand, the Maurice and Phyllis Paykel Trust, and the Maurice Wilkins Centre for Molecular Biodiscovery.

² Supported by British Heart Foundation Grant FS/05/054.

³ Supported by British Heart Foundation Grant PG/12/59/29795.

⁴ To whom correspondence may be addressed: School of Biological Sciences, University of Essex, Wivenhoe Park, Colchester CO4 3SQ, United Kingdom. E-mail: reyn@essex.ac.uk.

⁵ To whom correspondence may be addressed: School of Biological Sciences, University of Auckland, Auckland 1010, New Zealand. E-mail: dl.hay@auckland.ac.nz.

⁶ The abbreviations used are: AM, adrenomedullin; CGRP, calcitonin gene-related peptide; CLR, calcitonin-like receptor; ECD, extracellular domain; ECL, extracellular loop; GPCR, G protein-coupled receptor; RAMP, receptor activity-modifying protein; TM, transmembrane domain; Fmoc, *N*-(9-fluorenyl)methoxycarbonyl; RA, relative activity; PTH, parathyroid hormone; PDB, Protein Data Bank; DOPE, discrete optimized protein energy; GCGR, glucagon receptor; CRF1R, corticotropin releasing factor 1 receptor.

RAMP Effects on Adrenomedullin Receptors

RAMP2 results in embryonic lethality due to the development of hydrops fetalis and cardiovascular abnormalities (11–13). For example, *Adm*^{-/-} mice have small and disorganized hearts (13). Cardiomyocyte-specific RAMP2 knock-out disrupted cardiac metabolism and homeostasis by causing cardiac dilation and changes in mitochondrial structure (14). Furthermore, targeted RAMP2 overexpression in vascular smooth muscle suggests that the AM₁ receptor could protect against vascular remodeling invoked by prolonged hypertension (15).

RAMP3 knock-out mice give important insight into the likely role of the AM₂ receptor in cardiac biology. Unlike RAMP2 knock-out mice, these animals survive into old age and exhibit normal angiogenesis (12, 16). When challenged by crossing *Ramp3*^{-/-} with *RenTgMK* mice (a genetic model of angiotensin II-mediated cardiovascular disease), sex-dependent cardiovascular phenotypic differences emerge (*i.e.* renal failure and cardiac hypertrophy occur only in male mice) (16). A separate *Ramp3*^{-/-} model exhibited narrowed lymphatic vessels, impaired lymphatic drainage, and thus post-operative lymphedema and prolonged inflammation (17).

Thus, the AM₁ and AM₂ receptors have distinct roles. In animal models of cardiovascular disease, both the relative and absolute expression of the AM₁ and AM₂ receptor subunits change in different disease states. In the kidney of hypertensive rats, RAMP2 expression decreases, and RAMP3 expression increases (18). Each AM receptor is a potential drug target, and it is important to develop selective molecules for each receptor that can tease out the most beneficial receptor activity. For example, AM₁ receptor antagonists could be useful anti-angiogenic agents in cancer (9). In cardiovascular disease, either receptor could be a drug target. Receptor-selective molecules are urgently needed to tease out the role of each receptor and enable drug development efforts.

The AM receptors are compelling targets from a drug discovery perspective because of their biological effects and because they belong to the large GPCR superfamily of transmembrane proteins that are the cellular targets for 36% of all approved therapeutics (19). Peptide-binding class B GPCRs (including CLR) maintain the conserved heptahelical conformation observed across the wider superfamily with attendant intracellular loops, extracellular loops (ECLs), and a large extracellular domain (ECD) (20). Class B GPCR peptide ligands are known to interact with the ECD through their C terminus, with a second interaction of their N terminus with the juxtamembrane domain (the ECLs and the upper region of the transmembrane (TM) helices) that initiates receptor activation. However, the fact that the two AM receptors share a common GPCR (CLR) and the natural ligand (AM) makes minimal direct contact with the RAMP ECD (21) makes the design of receptor-specific drugs a challenge. Rational design of specific ligands would therefore benefit from improved knowledge of the full impact of RAMPs upon AM₁ and AM₂ receptor structure and function. In the pursuit of AM receptor agonists, a focus on the regions of CLR that trigger signaling is critical.

Here we explore how RAMPs affect the CLR juxtamembrane domain through extensive site-directed mutagenesis and molecular modeling. Our data suggest that RAMP2 and

RAMP3 each create unique CLR conformations that may be exploitable for the development of small molecule ligands.

Experimental Procedures

Materials—Human AM (AM(1–52)) was purchased from American Peptide (Sunnyvale, CA). Forskolin was from Tocris Bioscience (Wiltshire, UK). ALPHAscreen cAMP assay kits were from PerkinElmer Life Sciences. Poly-D-lysine-coated plates were from BD (Auckland, New Zealand). ¹²⁵I-AM(13–52) was from PerkinElmer Life Sciences.

Expression Constructs and Mutagenesis—Wild type (WT) human CLR with an N-terminal hemagglutinin (HA) epitope tag, human RAMP2 with an N-terminal FLAG epitope tag, and untagged human RAMP3 were used in this study (22, 23). The HA-CLR mutants and RAMP constructs have been described previously (24–26).

Cell Culture and Transfection—Culture of HEK293S cells was performed as described previously (23). Cells were counted using a Countess CounterTM (Invitrogen) and seeded at a density of 15,000 cells/well into 96-well poly-D-lysine-coated plates. For binding assays, 24-well plates were used (22). These were transiently transfected using polyethyleneimine as described previously (27).

Synthesis of Alanine-substituted AM(15–52) and Experiments with Phe¹⁸ AM—For experiments investigating the role of Phe¹⁸ in the AM peptide, we used an F18A AM(15–52) peptide, alongside a WT AM(15–52) control. As is evident from the data for full-length AM(1–52) and AM(15–52) (Tables 2 and 4), these peptides have equivalent function. The AM(15–52) peptides were synthesized by solid phase peptide synthesis using the Fmoc/*tert*-butyl method on a 0.1-mmol scale. Briefly, Rink amide aminomethyl resin was prepared (28), and the peptide was elongated using a CEM Liberty microwave peptide synthesizer (CEM Corp., Matthews, NC) using 5% (w/v) piperazine containing 0.1 M 6-chlorobenzotriazole in *N,N*-dimethylformamide as Fmoc deblocking reagent and *O*-(6-chlorobenzotriazol-1-yl)-*N,N,N',N'*-tetramethyluronium hexafluorophosphate, and *N,N*-diisopropylethylamine as coupling reagents using microwave settings as described previously (29). The peptides were cleaved from the resin with concomitant removal of side chain protecting groups with 94.0% trifluoroacetic acid, 1.0% triisopropylsilane, 2.5% water, and 2.5% 2,2'-(ethylene-dioxy)diethanethiol (v/v/v/v) for 2–3 h, precipitated with cold diethyl ether, recovered by centrifugation, dissolved in 50% aqueous acetonitrile containing 0.1% trifluoroacetic acid, and lyophilized. The crude peptides were dissolved in 0.1 M Tris (pH 8.1) at a concentration of 1 mg/ml, and the oxidation (disulfide formation) was allowed to proceed at room temperature open to air. Monitoring by reverse phase HPLC and/or LC-MS indicated that the reaction was typically complete within 1 day. The solution was acidified to pH 2 with 5 M HCl, purified directly by semipreparative reverse phase HPLC using a C18 Gemini (Phenomenex, Torrance, CA) column (10 × 250 mm) at a flow rate of 5 ml/min, and eluted using an appropriate gradient based on the analytical HPLC profile. Fractions containing the pure peptide were identified by electrospray mass spectrometry and/or HPLC, pooled, and lyophilized. All peptides were >95% pure as judged by integration of the HPLC chromatogram at 210 nm,

and peptide masses were confirmed by electrospray mass spectrometry.

cAMP Assays—We selected the mutants to study based on the boundaries of the ECLs according to our homology model of the calcitonin gene-related peptide (CGRP) receptor (CLR/RAMP1) (26, 30). CLR is predominantly G_s -coupled, so we characterized AM-stimulated cAMP signaling of alanine (or leucine, where natively alanine) mutants of CLR complexed with either RAMP2 or RAMP3. cAMP assays were performed as described previously using 1 mM isobutylmethylxanthine and a 15-min cell stimulation period (31). cAMP was then quantified using ALPHAscreen on a JANUS automated work station (PerkinElmer Life Sciences).

Analysis of Cell Surface Expression of Mutants by ELISA—CLR, RAMP2, and RAMP3 are inefficiently expressed on their own at the cell surface (32). However, when CLR is expressed with either RAMP, a functional AM_1 or AM_2 receptor is translocated to the cell surface. We determined expression levels of WT CLR/RAMP2 and CLR/RAMP3 heterodimers and cell surface expression of the mutant receptors as described previously, by measuring HA-CLR (33, 34). Due to the RAMP-dependent effects observed, we first ensured that each RAMP was capable of producing equivalent HA-CLR translocation to the cell surface: HA-CLR cell surface expression with ($A_{490} - A_{650/595}$) untagged RAMP1, 4.32 ± 0.31 ($n = 3$); Myc-RAMP1, 4.16 ± 0.22 ($n = 3$); untagged RAMP2, 2.81 ± 0.42 ($n = 3$); FLAG-RAMP2, 3.08 ± 0.38 ($n = 3$); or untagged RAMP3, 2.96 ± 0.36 ($n = 3$) (no significant differences by one-way analysis of variance). Thus, RAMP-specific effects of CLR mutations are unlikely to be due to an alteration in receptor density at the cell surface.

Radioligand Binding—AM binding assays were performed as described previously, displacing ^{125}I -AM(13–52) with unlabeled AM (22).

Data Analysis—All experiments were independently replicated at least three times, with two or three technical replicates in each experiment. Data analysis for cAMP assays was performed in GraphPad Prism version 6 (GraphPad Software, La Jolla, CA). Concentration-response curves were initially fitted to a four-parameter logistic equation; in all cases, the Hill slope was not significantly different from unity. Consequently, this was constrained to equal 1, the data were refitted to a three-parameter logistic equation, and pEC_{50} values were obtained. In order to determine E_{max} values for the mutant receptor curves, the data were normalized with respect to the fitted minimum and maximum of the WT curve. The combined normalized data sets were generated by combining the mean of the data points from the curves of each individual experiment. Variations in pEC_{50} between WT and mutant receptors were analyzed for statistical significance using an unpaired t test on the values obtained before curve normalization (*, $p < 0.05$; **, $p < 0.01$; ***, $p < 0.001$). E_{max} values expressed as a percentage of WT were analyzed similarly. A $\Delta \log pEC_{50}$ of ≥ 0.5 and a $\geq 30\%$ E_{max} difference (compared with WT) coupled to significance at the $p < 0.05$ level were used to identify residues with an unambiguous effect.

To further identify mutants that discriminated between AM_1 and AM_2 receptors, the differences in relative activity (RA) between the WT and mutant receptors were considered (35).

The $\log(RA)$ for each mutant and corresponding WT were calculated as $\log(\text{mutant } E_{max}/\text{mutant } EC_{50})$ and $\log(\text{WT } E_{max}/\text{WT } EC_{50})$. The mutant value was subtracted from the WT value to obtain $\Delta \log(RA)$. $\Delta \log(RA)$ values different from 0 were identified using multiple t tests with the false discovery rate set at 1%; differences between $\Delta \log(RA)$ at the AM_1 receptor and AM_2 receptor were investigated by a two-way analysis of variance followed by Sidak's multiple comparison test to compare individual means. Radioligand binding was analyzed in GraphPad Prism version 6 to a three-parameter logistic equation to obtain the pIC_{50} and maximum specific binding.

For ELISA, values were normalized to WT HA-CLR/RAMP as 100% and empty vector-transfected cells as 0%. Statistical significance between WT and mutants was determined using the 95% confidence interval.

AM Peptide Structure Model—The AM peptide structure (Fig. 1) was modeled from the known structures of its component parts (the disulfide-bonded region, the helical region, and the ECD region). The key stages in this modeling involved (i) the use of an in-house multiple-reference sequence alignment method tailored for aligning helices with low sequence identity (36) and (ii) the comparative modeling capabilities of PLOP (37). There is little structural information for full-length AM in its receptor-bound conformation, making structure-based sequence alignments difficult. Moreover, class B GPCR peptide ligands appear to lie in a number of distinct groups (38), so sequence alignment is not trivial. Consequently, separate alignments of the glucagon, GLP-1, PTH, and AM sequences were generated by ClustalX (39). The helical region of the AM peptide homologs, as indicated by the NMR structure (PDB code 2L7S) (40), was aligned to those of the equivalent helical region in the glucagon/GLP-1/PTH family of peptides using an in-house multiple-reference method tailored for aligning helices with low sequence identity (36) that is a development of the methods of reference (41). The alignment is given in Fig. 1A; the alignment scores shown in Fig. 1B (and Fig. 1C) give strong support for the proposed alignment over the only plausible alternative involving a shift left of the AM helix by 4 positions. The AM/CLR/RAMP2 (PDB code 4RWF) ECD (21), the GLP-1/exendin-4 structure (PDB code 3C59) (42), and the glucagon model structure (43) were structurally aligned using the SALIGN module of MODELER (44) (Fig. 1D), from which a template was constructed using Asp³⁵-Tyr⁵² from the AM x-ray structure and Thr⁷-Tyr¹³ of the glucagon model peptide structure, which was preferred over the corresponding (Thr⁷)-Asp⁹-Gln¹³ of exendin-4 because the angle was more appropriate for peptide binding to the TM bundle. The missing loop was inserted using the comparative modeling, loop modeling, and minimization capabilities of PLOP (37) based on the alignment in Fig. 1F. The N terminus, taken from Woolley *et al.* (26), was added by structural alignment of the common helical domain using VMD (45), again using the alignment in Fig. 1A. The resulting peptide structure of AM(15–52) (structurally aligned to the CLR ECD) is shown in Fig. 1E.

AM_1 and AM_2 Receptor Models—Comparative AM_1 and AM_2 receptor models were generated using MODELER version 9.12 (44), essentially from two x-ray structures, namely the AM CLR-RAMP2 ECD complex (21) (PDB code 4RWF) and the

RAMP Effects on Adrenomedullin Receptors

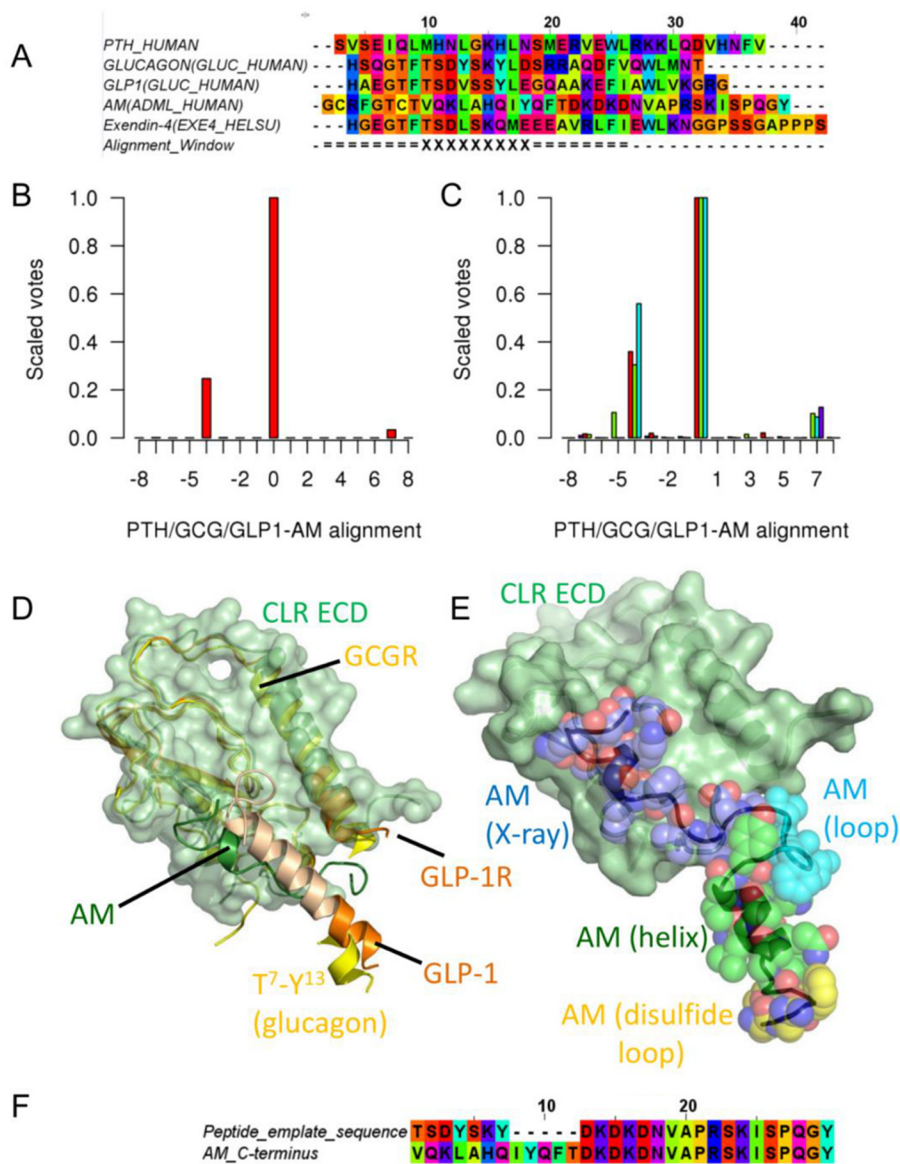


FIGURE 1. Modeling the AM peptide. *A*, selected class B peptide alignments. Homologs of each of PTH, glucagon, and GLP-1 were aligned against AM homologs in a multireference profile alignment, as described by Lock *et al.* (36), over the helical region denoted *X*. *B*, the multireference alignment scores. Alignment 0, corresponding to the alignment in *A*, has the highest score; the next highest score (alignment -4) corresponds to moving the AM helix 4 residues to the left, but this alternative score is low. *C*, as for *B* but missing PTH (red), glucagon (green), or GLP-1 (cyan); the results are presented as a control. *D*, a structural alignment of CLR (light green surface, schematic)/AM(35–52) (dark green schematic), GLP-1R (orange schematic)/extendin-4 (wheat/orange schematic), and GCGR (yellow schematic)/glucagon Thr⁷–Tyr¹³ (yellow). The AM(23–52) comparative modeling template was taken from AM(35–52) and glucagon Thr⁷–Tyr¹³. The extendin-4 is largely wheat-colored, but the region corresponding to Thr⁷–Tyr¹³ of glucagon is orange. *E*, the final AM(16–52) structure (black schematic, used as one of the templates for modeling the AM receptor) structurally aligned to the CLR ECD. The various components of AM are shown as color-coded transparent spheres: yellow, carbon atoms (disulfide-bonded loop); green, carbon atoms (helix); cyan, carbon atoms (loop); blue, carbon atoms (from the original x-ray structure). The final structure is very similar to this initial template structure. *F*, the alignment for the comparative modeling of AM(23–52).

glucagon receptor (GCGR) TM domain (43) (PDB code 4L6R). The GCGR was preferred over the corticotropin-releasing factor 1 receptor (CRF1R) TM structure because of its overall conformation and compatibility with the full GCGR model (43), but part of the superior quality CRF1R structure (as denoted by ERRAT (46)) was used in subsequent refinement. In addition, model structures for the full GCGR model (43) containing only Ser⁸–Asp¹⁵ of glucagon (*cf.* Fig. 1*D*), the full-length AM peptide (Fig. 1*E*), CGRP(1–7) docked to an active model of CLR (26), and a model of the RAMP1 TM helix docked to TM7 were used (Fig. 2). The active character of the model was also imposed by including TM5–6 of an active CLR model derived

from the β_2 -adrenergic receptor active complex (47); this template also contained the C-terminal peptide of the G protein, G_s (Arg³⁷³–Leu³⁹⁴). Each of these structural templates contained information on part but not all of the desired structure and was linked via a global alignment (Fig. 3). In addition, we also included short N- and C-terminal extensions (6 and 5 residues, respectively) to the RAMP TM helix and the RAMP ECD to prevent the linker between them from becoming entangled in the bulk of the receptor. Within this alignment, the position of the gap in the CLR sequence between the ECD and TM1 relative to the longer human glucagon receptor sequence was determined by analysis of gaps in similar subsets within the

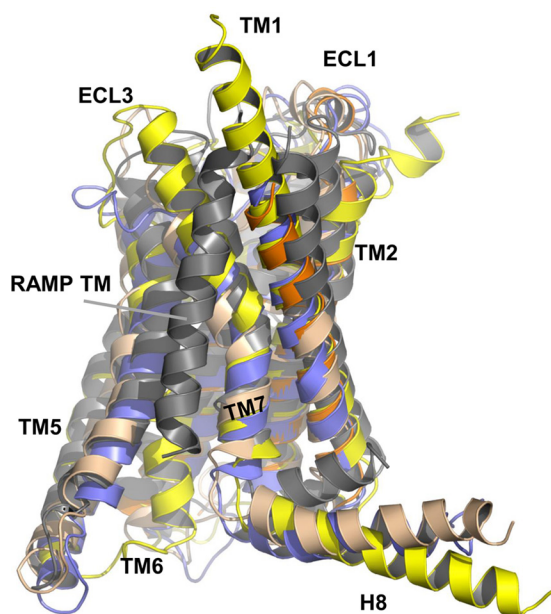


FIGURE 2. The template structure of RAMP docked to an active model of CLR. The template structure (gray) was generated as follows. The length of the TM helix for RAMP1 is given as 21 residues by UniProt, but this is too short for a tilted helix to span the membrane. Consequently, for RAMP1, helices of lengths 26, 28, and 30 residues were constructed using Maestro, commencing at Ser¹¹⁷, Pro¹¹⁵, and Asp¹¹³, respectively. For RAMP2, helices of length 24, 26, and 28 residues were constructed, commencing at Asp¹⁴⁴, Pro¹⁴², and Asp¹⁴⁰, respectively. For RAMP3, helices of lengths 25, 26, and 28 residues were constructed, commencing at Asp¹¹⁶, Pro¹¹⁵, and Asp¹¹³, respectively. The helices were docked using the Cluspro, PatchDock, and SwarmDock servers to two active models of the CLR transmembrane helical bundle (six docking experiments) (30, 65–67); the active explicit membrane CLR model has been shown to be in very good agreement with the x-ray crystal structures of the GPCR and CRF1R (26). Results from each server that were not compatible with the membrane topology were eliminated, and the remaining viable solutions were clustered. Representative solutions were then refined and rescored using the FireDock server (so that poses generated by the different servers are treated equally) (68, 69). The three best poses (on the basis of lowest energy and geometry consensus) were then docked using RosettaDock (70–72). The consensus result showed a preference for the helix to dock to TM7 of the active receptor, in agreement with experimental results that indicate an interaction with TM6/7 (60). The active AM₁ (light blue) and AM₂ (wheat) model TM domains, the inactive GPCR (yellow), and TM1–TM4 of inactive CRF1R (orange) structures, superimposed over TM1, TM2, TM3, the top of TM4 (because of irregularities in the GPCR x-ray structure; *c.f.* CRF1R), and TM7, are also shown. TM5, TM6, and the top of TM7 were omitted from the fitting because of differences in active and inactive structures in this region. All root mean square deviations were <2 Å.

glucagon multiple-sequence alignment (48). Two thousand models were generated, and the model having the lowest (best) DOPE score was chosen for further refinement. ECL1 was refined using MODELER from TM1–4 of a CLR model derived from the CRF1R structure in which variability (30, 49, 50) was used to orient the CLR ECL1 helix, as in a recent GLP-1 receptor model (51). The ECLs and the RAMP linker (here defined as the region connecting the extracellular helical domain and the TM helix (*i.e.* residues Val¹³⁴–Leu¹⁴⁷ for RAMP2 and Val¹⁰⁶–Leu¹¹⁹ for RAMP3)) were refined using PLOP, which has been shown to perform well in GPCR loop modeling (37); this refinement removed any bias introduced by the extensions. The final models were minimized using PLOP (37).

Druggability was assessed using the PockDrug (52, 53) and DoGSiteScorer Web servers (54); pocket hull volumes (which include atoms within the druggable binding pockets) were also

determined using PockDrug; distances were measured using the PyMOL Molecular Graphics System (version 1.7.4; Schrödinger, LLC, New York), which was also used for image generation. The models are available as supplemental models 1 and 2.

Results

Receptor Cell Surface Expression—The cell surface expression levels of the WT AM₁ and AM₂ receptors were not significantly different (see “Experimental Procedures”). The cell surface expression of all mutant receptors showed very few significant differences compared with WT (Table 1). L351A and E357A CLR showed an ≥80% reduction of cell surface expression with both RAMPs, suggesting that these mutations caused the receptors to fail quality control processes prior to reaching the cell surface. Further data for these mutants is not discussed.

Functional Analysis of Receptor Mutations—We assayed a total of 68 CLR mutants with RAMP2 and with RAMP3. All results are reported in Tables 2 and 3. cAMP data for selected mutants, which illustrate a breadth of effects, are shown in Figs. 4 and 5. The mutations could in principle change either the affinity of binding of AM or its ability to activate the receptor (efficacy). Efficacy can be estimated to some extent from E_{max} , but this is limited by receptor reserve. Furthermore, for many mutants, we cannot measure affinity directly because the only radioligand available to us is the agonist, ¹²⁵I-AM, which will not give detectable binding once its affinity goes below around 10 nM. The EC₅₀ describes potency but does not provide a ready means for identifying mutants that alter efficacy as well as affinity. Accordingly, we have used $\Delta\log(\text{RA})$ (see “Experimental Procedures”) as a simple parameter to characterize the effect of the mutations in functional assays; where appropriate, we supplement this with observations on E_{max} or EC₅₀. Using this, we describe below our major observations, categorized according to the effect of the mutation. We have also conducted radioligand binding assays using ¹²⁵I-AM on selected mutants to provide additional information (Fig. 6).

There was a core subset of six residues that were important for the function of the AM₁ and AM₂ receptors (Ala¹⁹⁹, Asp²⁸⁰, Ile²⁸⁴, Thr²⁸⁸, Phe³⁴⁹, and Tyr³⁶⁵), producing shared changes in pEC₅₀, E_{max} or $\Delta\log(\text{RA})$. We define all of these six as having common effects (Fig. 4). These residues are situated within ECL2 and the TM6–ECL3–TM7 juxtamembrane region, along with A199L in TM2.

A further 10 mutations had an effect at both AM receptors, but the nature of the effect differed between the two receptors (Leu¹⁹⁵, Val¹⁹⁸, Cys²¹², Lys²¹³, Arg²⁷⁴, Trp²⁸³, Ile³⁵², Pro³⁵³, Trp³⁵⁴, and Ala³⁶¹). These are defined as residues with common but differential effects (Fig. 5). L195A in TM2, C212A at the ECL1–TM3 boundary, and P353A at the TM6–ECL3 boundary abolished AM-mediated cAMP production at the AM₁ receptor, whereas K213A reduced this by 80%. For C212A, there was a trend for the radioligand binding to be modestly reduced at the AM₁ receptor but enhanced at the AM₂ receptor, consistent with a differential effect of this mutation at both receptors (Fig. 6). The corresponding mutations in the AM₂ receptor were less deleterious. I352A and W354A mutations gave very similar changes in $\Delta\log(\text{RA})$, and radioligand binding shows a

TABLE 1

Cell surface expression of AM₁ and AM₂ receptors expressed as a percentage of the wild type receptorData are mean ± S.E. of *n* = 3–4 individual experiments. *95% confidence interval does not include 100%.

	TM2-ECL1-TM3			TM4-ECL2-TM5			TM6-ECL3-TM7	
	AM ₁ receptor	AM ₂ receptor		AM ₁ receptor	AM ₂ receptor		AM ₁ receptor	AM ₂ receptor
	%	%		%	%		%	%
L195A	91.2 ± 2.08	81.4 ± 25.9	A271L	118.8 ± 13.2	118.8 ± 20.6	F349A	98.5 ± 11.3	93.9 ± 22.5
T196A	94.9 ± 17.8	90.5 ± 20.1	I272A	115.9 ± 15.6	64.1 ± 23.5	V350A	104.2 ± 8.06	106.5 ± 33.4
A197L	111.4 ± 7.28	85.9 ± 21.2	A273L	112.3 ± 11.6	107.7 ± 6.74	L351A	9.75 ± 3.17*	21.9 ± 12.3*
V198A	105.8 ± 14.1	84.3 ± 19.0	R274A	98.1 ± 17.3	107.2 ± 14.4	I352A	68.9 ± 10.2*	121.2 ± 13.7
A199L	99.8 ± 7.56	136.7 ± 76.6	S275A	77.3 ± 10.1	113.0 ± 25.3	P353A	94.2 ± 8.95	104.0 ± 23.8
N200A	100.1 ± 6.69	48.4 ± 8.62	L276A	73.8 ± 10.2	110.3 ± 21.7	W354A	85.9 ± 9.30	103.7 ± 24.0
N201A	81.9 ± 15.9	38.9 ± 13.4	Y277A	94.0 ± 7.26	132.4 ± 23.0	R355A	114.7 ± 13.0	86.5 ± 11.8
Q202A	94.8 ± 1.92	83.2 ± 10.2	Y278A	75.8 ± 27.6	154.1 ± 27.1	P356A	101.3 ± 3.59	87.6 ± 13.3
A203L	95.5 ± 9.67	72.1 ± 18.4	N279A	97.0 ± 6.30	96.8 ± 17.0	E357A	17.2 ± 4.85*	15.1 ± 9.97*
L204A	98.3 ± 2.83	114.0 ± 15.8	D280A	155.8 ± 68.9	126.1 ± 16.8	G358A	108.2 ± 7.72	85.7 ± 9.81
V205A	117.3 ± 6.49	88.7 ± 13.1	N281A	108.1 ± 2.90	119.9 ± 2.97	K359A	99.6 ± 2.63	76.3 ± 11.9
A206L	92.9 ± 8.45	91.4 ± 13.1	C282A	64.9 ± 16.8	100.7 ± 11.7	I360A	85.8 ± 3.81	82.5 ± 7.48
T207A	99.9 ± 1.52	82.2 ± 15.5	W283A	107.7 ± 11.9	100.4 ± 13.4	A361L	102.2 ± 3.45	83.1 ± 8.75
N208A	98.6 ± 1.02	111.5 ± 18.4	I284A	67.1 ± 8.80	107.6 ± 26.2	E362A	103.8 ± 6.14	75.4 ± 4.93
P209A	100.3 ± 5.96	118.6 ± 34.5	S285A	86.1 ± 20.2	124.7 ± 31.6	E363A	103.0 ± 2.74	75.6 ± 4.22
V210A	100.4 ± 5.63	88.2 ± 15.0	S286A	93.2 ± 12.9	104.7 ± 15.0	V364A	94.0 ± 2.74	100.5 ± 12.5
S211A	97.5 ± 3.73	95.4 ± 18.7	D287A	77.4 ± 13.4	107.3 ± 7.33	Y365A	92.5 ± 6.21	121.3 ± 24.5
C212A	119.0 ± 25.1	93.6 ± 22.1	I288A	94.8 ± 23.5	90.0 ± 7.14	D366A	107.5 ± 4.33	103.1 ± 19.4
K213A	131.3 ± 33.1	84.3 ± 21.3	H289A	93.1 ± 16.2	95.7 ± 12.9	Y367A	110.0 ± 2.03	106.2 ± 16.4
V214A	87.5 ± 9.71	86.6 ± 17.9	L290A	102.5 ± 2.45	98.6 ± 7.36	I368A	90.8 ± 15.2	118.6 ± 24.7
S215A	86.2 ± 10.7	84.5 ± 17.3	L291A	103.5 ± 7.54	130.8 ± 10.3	M369A	82.8 ± 13.9	108.2 ± 25.1
Q216A	95.7 ± 2.47	124.9 ± 23.7	Y292A	83.5 ± 7.47	176.5 ± 40.6			
F217A	101.8 ± 7.45	99.0 ± 12.0	I293A	99.2 ± 1.44	107.9 ± 12.5			
			I294A	103.2 ± 14.7	102.8 ± 29.8			

similar reduction in specific binding for I352A at both receptors (Fig. 6). However, in both cases, the effects on E_{\max} were more marked at the AM₁ receptor, so these have been included as common but differential residues. Whereas V198A showed only a small difference in $\Delta\log(\text{RA})$, it significantly increased E_{\max} at the AM₂ receptor but not the AM₁ receptor. A361L was a difficult mutant to characterize; whereas the E_{\max} is reduced at both the AM₁ and AM₂ receptors, the changes in $\Delta\log(\text{RA})$ were of opposing directions.

Five of the 68 mutants had more pronounced differential effects between the receptors. These are referred to as differential residues (Fig. 5). A271L, Y277A, Y278A, N279A, and C282A all increased $\Delta\log(\text{RA})$ at the AM₁ receptor but had no significant effect at the AM₂ receptor. For Y277A, radioligand binding was substantially reduced at the AM₁ receptor but retained at the AM₂ receptor, consistent with a differential effect of this mutation at both receptors. C282A binding was unchanged at the AM₁ receptor but showed a trend to be enhanced at the AM₂ receptor (Fig. 6). In addition, for Y367A, we observed a decrease in pEC_{50} at the AM₂ receptor but no effect at the AM₁ receptor. Although the differences in E_{\max} at either receptor did not reach statistical significance, the effect was opposite with an increase at the AM₂ receptor and a decrease at the AM₁ receptor. This is an atypical mutation because the effect is greater at the AM₂ receptor.

Overall Description of the AM₁ and AM₂ Receptor Models—To assist in data interpretation, we generated AM₁ and AM₂ receptor models, which we understand to be the first models of a full-length GPCR in complex with a RAMP (Fig. 7, A and B). The RAMP TM helix lies between TM6 and TM7 of CLR with-

out inducing strain in the sequence joining the RAMP ECD to the TM (the RAMP linker). The predicted arrangement of the TM helices forms a conical pocket (the peptide binding site) into which the disulfide loop of the AM peptide docks (Fig. 7, C and D). ECL boundaries are very similar to those in the CGRP receptor (26) and those of other class B GPCR x-ray structures (43, 50).

In the AM peptide model, residues 15–21 form a disulfide loop, residues 22–31 are helical (40), and residues 35–52 adopt the largely non-helical structure bound to the ECD of the AM₁ receptor (21); the remaining residues (positions 33–41) form a loop, creating the AM structure. The model therefore rationalizes previous work on the degree of helicity within AM (Fig. 1E). The RAMP2 linker (residues Val¹³⁴–Leu¹⁴⁷ between the ECD and the TM region) is displaced relative to that of RAMP3, lies closer to the peptide binding pocket than does RAMP3, and is predicted by the models to interact with ECL3 and the top of TM7 of CLR (Figs. 7 and 9).

The electrostatic potential of AM in its proposed bound conformation (Fig. 8, A and B) is largely positive because AM carries a charge of +4. The electrostatic potential of CLR in the absence of RAMP and AM is largely positive or neutral (Fig. 8, C and D). Both RAMP2 and RAMP3 convey an advantage in binding the positive AM because they switch this potential in the conical TM pocket and particularly on the ECD to more negative values, which will aid in binding the positively charged AM (Fig. 8, E and F). RAMP3 gives rise to the most negative ECD electrostatic potential.

Detailed Comparison between AM₁ and AM₂ Receptor Models—Overall, the ECL2 conformation is similar between the two models, consistent with the observation that many of

FIGURE 3. **The alignment for comparative modeling.** The alignment was generated by structural alignment of the templates using the SALIGN module of MODELER and refined using Jalview (73). The residues are color-coded according to their properties as follows: blue, positive; red, negative or small polar; purple, polar; green large hydrophobic; yellow, small hydrophobic; cyan, polar, aromatic. This corresponds to the “Taylor” scheme, as implemented in Jalview. The extracellular loops are denoted by gray shading and the loop number.

RAMP Effects on Adrenomedullin Receptors

TABLE 2

Pharmacological parameters of cAMP accumulation for the AM receptors when stimulated by AM

, $p < 0.05$; *, $p < 0.01$; *****, $p < 0.001$ versus WT, by unpaired *t* test except for $\Delta\log(\text{RA})$, where the comparison is between AM₁ and AM₂ receptors by two-way analysis of variance followed by Sidak's multiple comparison test. Common residues are in boldface type, common-differential residues are in boldface italic type, and differential residues are in italic type.

	AM ₁ receptor					<i>n</i>	AM ₂ receptor					<i>n</i>
	WT pEC ₅₀	Mutant pEC ₅₀	$\Delta\log$ pEC ₅₀	<i>E</i> _{max} (%WT)	$\Delta\log(\text{RA})$		WT pEC ₅₀	Mutant pEC ₅₀	$\Delta\log$ pEC ₅₀	<i>E</i> _{max} (%WT)	$\Delta\log(\text{RA})$	
TM2												
<i>LI95A</i>	9.28 ± 0.10	<6	>2.00	No curve ^a	-	5	9.11 ± 0.16	7.40 ± 0.17***	1.71	65.3 ± 11.3*	1.90 ± 0.25 ^{b,c}	5
<i>T196A</i>	8.94 ± 0.13	8.95 ± 0.03	-0.01	119.5 ± 23.5	-0.09 ± 0.16	3	8.90 ± 0.19	8.66 ± 0.19	0.24	116.5 ± 20.4	0.17 ± 0.28	3
<i>A197L</i>	8.91 ± 0.25	8.61 ± 0.13	0.30	90.4 ± 6.32	0.34 ± 0.28	4	9.19 ± 0.14	8.90 ± 0.11	0.29	136.9 ± 30.1	0.15 ± 0.20	3
<i>VI98A</i>	9.13 ± 0.11	8.32 ± 0.15***	0.81	74.5 ± 12.2	0.94 ± 0.20 ^b	7	9.41 ± 0.14	8.64 ± 0.19*	0.77	160.6 ± 26.16*	0.56 ± 0.25	3
ECL1												
<i>A199L</i>	9.14 ± 0.12	8.10 ± 0.23**	1.04	55.4 ± 8.56**	1.29 ± 0.28 ^b	6	9.29 ± 0.16	7.98 ± 0.20**	1.31	88.6 ± 9.46	1.36 ± 0.26	4
<i>N200A</i>	9.11 ± 0.16	9.55 ± 0.10	0.44	80.9 ± 17.4	-0.35 ± 0.21	3	9.16 ± 0.14	9.57 ± 0.22	-0.41	69.3 ± 3.75***	-0.25 ± 0.26	3
<i>N201A</i>	9.02 ± 0.16	8.70 ± 0.18	0.32	89.8 ± 4.70	0.37 ± 0.24	4	9.14 ± 0.10	8.50 ± 0.22	0.64	133.3 ± 36.3	0.52 ± 0.27	3
<i>Q202A</i>	9.00 ± 0.07	9.15 ± 0.09	-0.15	82.9 ± 11.1	-0.069 ± 0.13	4	9.14 ± 0.10	9.30 ± 0.13	-0.16	184.4 ± 40.3	-0.43 ± 0.19	3
<i>A203L</i>	9.27 ± 0.08	9.14 ± 0.08	0.13	82.5 ± 6.92*	0.21 ± 0.12	5	9.14 ± 0.10	9.14 ± 0.08	0.00	207.5 ± 57.6	-0.32 ± 0.17	3
<i>L204A</i>	8.93 ± 0.04	8.62 ± 0.03**	0.31	98.9 ± 5.36	0.31 ± 0.06	3	9.42 ± 0.29	8.89 ± 0.16	0.53	145.7 ± 24.9	0.37 ± 0.34	3
<i>V205A</i>	9.10 ± 0.06	8.67 ± 0.14*	0.43	79.9 ± 16.8	0.53 ± 0.30.18	4	9.42 ± 0.29	9.10 ± 0.10	0.32	135.2 ± 34.7	0.19 ± 0.32	3
<i>A206L</i>	9.30 ± 0.08	8.93 ± 0.09*	0.37	113.3 ± 17.8	0.32 ± 0.14	4	9.42 ± 0.29	9.33 ± 0.14	0.09	118.2 ± 43.4	0.02 ± 0.36	3
<i>T207A</i>	9.10 ± 0.06	9.08 ± 0.16	0.02	87.6 ± 2.59*	0.077 ± 0.17	4	9.41 ± 0.05	9.21 ± 0.05	0.20	81.7 ± 14.2	0.29 ± 0.10	4
<i>N208A</i>	8.97 ± 0.06	8.73 ± 0.10	0.24	84.9 ± 10.7	0.31 ± 0.13	5	9.41 ± 0.05	8.82 ± 0.04***	0.59	105.4 ± 39.8	0.57 ± 0.18	4
<i>P209A</i>	8.99 ± 0.02	8.63 ± 0.09**	0.36	109.0 ± 13.4	0.32 ± 0.11	4	9.41 ± 0.05	8.88 ± 0.15*	0.53	107.2 ± 40.2	0.50 ± 0.23	4
<i>V210A</i>	9.19 ± 0.06	9.03 ± 0.14	0.16	74.9 ± 5.17**	0.29 ± 0.16	4	9.25 ± 0.10	9.03 ± 0.08	0.22	133.3 ± 18.9	0.10 ± 0.14	3
<i>S211A</i>	9.09 ± 0.10	8.97 ± 0.11	0.12	103.5 ± 12.1	0.11 ± 0.15	5	9.25 ± 0.10	9.10 ± 0.03	0.15	143.8 ± 66.6	-0.01 ± 0.23	3
TM3												
<i>C212A</i>	9.04 ± 0.21	<6	>2.00	No curve	-	6	9.20 ± 0.07	8.59 ± 0.15**	0.61	91.51 ± 18.7	0.65 ± 0.19 ^c	6
<i>K213A</i>	9.22 ± 0.09	8.05 ± 0.09***	1.17	21.2 ± 7.38***	1.84 ± 0.204 ^b	5	9.14 ± 0.08	8.31 ± 0.07***	0.83	97.7 ± 8.43	0.84 ± 0.11 ^b	5
<i>V214A</i>	9.11 ± 0.12	9.01 ± 0.17	0.10	89.4 ± 7.11	0.15 ± 0.21	5	9.14 ± 0.11	9.14 ± 0.17	0.00	98.7 ± 9.12	0.01 ± 0.21	4
<i>S215A</i>	8.90 ± 0.12	8.81 ± 0.06	0.09	99.3 ± 1.87	0.093 ± 0.13	4	9.21 ± 0.12	9.22 ± 0.21	0.01	111.4 ± 13.8	-0.06 ± 0.25	3
<i>Q216A</i>	9.00 ± 0.12	9.60 ± 0.24	-0.6	100.2 ± 20.1	-0.60 ± 0.28	5	9.45 ± 0.14	9.42 ± 0.15	0.03	84.9 ± 7.41	0.10 ± 0.21	3
<i>F217A</i>	9.19 ± 0.03	8.82 ± 0.11**	0.37	97.3 ± 18.8	0.38 ± 0.14	7	9.41 ± 0.11	8.99 ± 0.15	0.44	100.3 ± 17.0	0.42 ± 0.20	5
TM4												
<i>A271L</i>	9.27 ± 0.14	8.33 ± 0.23**	0.94	71.4 ± 9.83*	1.09 ± 0.28	5	9.41 ± 0.09	9.16 ± 0.18	0.25	98.8 ± 33.7	0.26 ± 0.25	5
<i>I272A</i>	9.31 ± 0.18	9.65 ± 0.18	-0.34	151.6 ± 87.8	-0.52 ± 0.36	6	9.41 ± 0.09	9.42 ± 0.08	0.01	94.3 ± 18.1	0.02 ± 0.15	5
<i>A273L</i>	8.96 ± 0.14	8.91 ± 0.09	0.05	147.4 ± 42.7	-0.12 ± 0.215	4	9.26 ± 0.10	9.15 ± 0.09	0.11	100.4 ± 9.90	0.11 ± 0.14	4
<i>R274A</i>	9.51 ± 0.18	7.32 ± 0.14***	2.19	17.7 ± 5.01***	2.94 ± 0.26 ^b	5	9.24 ± 0.08	8.24 ± 0.11***	1.00	31.6 ± 10.1***	1.50 ± 0.19 ^{b,***}	5
ECL2												
<i>S275A</i>	9.29 ± 0.13	9.39 ± 0.21	-0.10	103.3 ± 18.2	-0.11 ± 0.26	5	9.30 ± 0.15	9.23 ± 0.22	-0.10	114.9 ± 22.6	0.01 ± 0.28	5
<i>L276A</i>	9.29 ± 0.17	9.23 ± 0.15	0.06	96.8 ± 18.0	0.074 ± 0.24	4	9.30 ± 0.15	9.34 ± 0.16	-0.04	70.2 ± 12.4	0.11 ± 0.23	4
<i>Y277A</i>	9.51 ± 0.13	8.79 ± 0.19*	0.72	33.3 ± 8.98***	1.20 ± 0.26 ^b	7	9.35 ± 0.09	9.23 ± 0.05	0.12	113.7 ± 21.2	0.06 ± 0.13**	5
<i>Y278A</i>	9.54 ± 0.13	8.45 ± 0.13***	1.13	55.9 ± 9.33***	1.34 ± 0.20 ^b	7	9.34 ± 0.12	8.92 ± 0.09	0.42	106.0 ± 29.5	0.39 ± 0.19	5
<i>N279A</i>	9.04 ± 0.10	8.53 ± 0.31	0.25	21.7 ± 25.9	1.17 ± 0.614	4	9.45 ± 0.10	9.17 ± 0.10	0.28	95.6 ± 11.8	0.30 ± 0.15	4
D280A												
<i>N281A</i>	9.29 ± 0.08	8.39 ± 0.08***	0.90	73.6 ± 7.61**	1.03 ± 0.12 ^b	6	9.56 ± 0.07	8.31 ± 0.26**	1.25	93.7 ± 19.0	1.28 ± 0.28 ^b	5
<i>C282A</i>	9.32 ± 0.08	9.26 ± 0.10	0.06	128.7 ± 16.9	-0.05 ± 0.14	5	9.64 ± 0.10	9.44 ± 0.19	0.20	143.9 ± 16.7	0.04 ± 0.22	4
<i>W283A</i>	9.09 ± 0.05	8.15 ± 0.21**	0.94	48.5 ± 10.2***	1.25 ± 0.23 ^b	6	9.10 ± 0.11	8.88 ± 0.18	0.22	117.3 ± 16.7	0.15 ± 0.22*	5
<i>W283A</i>	9.19 ± 0.13	6.96 ± 0.17***	2.23	25.9 ± 11.7***	2.82 ± 0.29 ^b	5	9.54 ± 0.08	7.96 ± 0.10***	1.58	71.7 ± 27.5	1.72 ± 0.21 ^{b,c}	5
I284A												
<i>S285A</i>	8.97 ± 0.11	6.75 ± 0.35**	2.02	35.2 ± 7.25***	2.67 ± 0.38 ^b	5	9.08 ± 0.12	7.36 ± 0.21***	1.72	51.8 ± 18.4**	2.01 ± 0.29 ^b	5
<i>S286A</i>	9.33 ± 0.07	9.02 ± 0.08	0.31	196.7 ± 113.9	0.02 ± 0.27	4	9.60 ± 0.09	9.37 ± 0.11	0.23	157.7 ± 52.8	0.03 ± 0.20	5
<i>D287A</i>	9.16 ± 0.27	9.31 ± 0.20	-0.15	99.2 ± 16.8	-0.15 ± 0.34	4	9.45 ± 0.18	9.66 ± 0.11	-0.19	71.4 ± 26.4	-0.06 ± 0.26	3
<i>D287A</i>	9.26 ± 0.05	9.51 ± 0.47	-0.25	105.3 ± 34.5	-0.27 ± 0.49	4	9.31 ± 0.05	9.12 ± 0.12	0.19	104.5 ± 18.8	0.17 ± 0.15	4
T288A												
<i>H289A</i>	9.15 ± 0.13	8.37 ± 0.05***	0.78	51.4 ± 3.32***	1.07 ± 0.14 ^b	4	9.60 ± 0.09	8.97 ± 0.11***	0.63	78.46 ± 14.6	0.74 ± 0.16	4
<i>L290A</i>	9.09 ± 0.04	9.12 ± 0.13	-0.03	118.7 ± 8.74	-0.10 ± 0.14	4	9.58 ± 0.26	9.74 ± 0.25	-0.16	298.8 ± 143.9	-0.64 ± 0.42	5
<i>L291A</i>	8.96 ± 0.14	8.83 ± 0.09	0.13	190.9 ± 84.2	-0.15 ± 0.25	4	9.26 ± 0.09	8.97 ± 0.08	0.29	94.4 ± 13.8	0.32 ± 0.14	3
<i>L291A</i>	9.09 ± 0.04	8.62 ± 0.14*	0.47	136.7 ± 45.1	0.33 ± 0.20	4	9.18 ± 0.12	8.83 ± 0.15	0.35	125.1 ± 32.2	0.25 ± 0.22	6
TM5												
<i>Y292A</i>	8.96 ± 0.14	8.54 ± 0.06*	0.42	91.2 ± 18.9	0.46 ± 0.18	4	9.32 ± 0.10	8.67 ± 0.17*	0.65	135.1 ± 42.2	0.52 ± 0.24	4
<i>I293A</i>	8.97 ± 0.04	9.20 ± 0.07*	-0.28	93.2 ± 29.6	-0.20 ± 0.16	4	9.01 ± 0.07	9.13 ± 0.02	-0.12	121.8 ± 23.1	-0.21 ± 0.11	3
<i>I294A</i>	9.09 ± 0.04	8.83 ± 0.21	0.26	147.5 ± 53.5	0.09 ± 0.26	4	9.18 ± 0.12	9.12 ± 0.14	0.06	128.3 ± 19.1	-0.05 ± 0.19	5
TM6												
<i>F349A</i>	9.01 ± 0.11	8.72 ± 0.11	0.29	21.5 ± 1.81***	0.96 ± 0.16 ^b	5	9.14 ± 0.05	8.61 ± 0.07**	0.53	24.0 ± 9.13***	1.15 ± 0.19 ^b	5
<i>V350A</i>	8.86 ± 0.28	8.72 ± 0.07	0.14	63.7 ± 4.94***	0.34 ± 0.29	4	9.14 ± 0.05	8.87 ± 0.34	0.27	65.8 ± 17.3	0.45 ± 0.36	4
<i>L351A</i>	9.15 ± 0.10	No curve	>3	No Curve	-	4	9.09 ± 0.06	No Curve	>3	No Curve	-	3
<i>I352A</i>	9.01 ± 0.11	8.28 ± 0.27*	0.73	37.7 ± 9.87***	1.15 ± 0.31	5	9.40 ± 0.08	8.46 ± 0.10***	0.94	86.9 ± 30.1	1.00 ± 0.20 ^b	5
<i>P353A</i>	9.07 ± 0.13	No Curve	>3	No Curve	-	5	9.42 ± 0.09	8.49 ± 0.06***	0.91	47.1 ± 9.19***	1.26 ± 0.14 ^{b,c}	5
<i>W354A</i>	9.29 ± 0.06	8.50 ± 0.12***	0.79	37.2 ± 7.38***	1.22 ± 0.16 ^b	5	9.40 ± 0.08	8.59 ± 0.13***	0.81	112.4 ± 17.5	0.76 ± 0.17 ^b	5
<i>R355A</i>	9.13 ± 0.08	9.50 ± 0.12*	-0.37	80.4 ± 7.97*	-0.27 ± 0.15	4	9.27 ± 0.26	9.89 ± 0.03	-0.62	91.0 ± 18.6	-0.58 ± 0.28	3
<i>P356A</i>	9.15 ± 0.10	8.99 ± 0.10	0.16	40.4 ± 3.66***	0.55 ± 0.15	4	9.34 ± 0.20	9.12 ± 0.29	0.22	60.0 ± 23.1	0.44 ± 0.39	4
ECL3												
<i>E357A</i>	9.00 ± 0.08	No Curve	>3	No Curve	-	4	9.23 ± 0.26	No Curve	>3	No Curve	-	3
<i>G358A</i>	9.09 ± 0.11	9.06 ± 0.11	0.03	104.5 ± 5.46	0.01 ± 0.16	4	8.79 ± 0.14	8.84 ± 0.27	-0.05	80.9 ± 55.3	0.04 ± 0.42	3
<i>K359A</i>	9.09 ± 0.11	9.19 ± 0.10	-0.10	107.5 ± 4.28	-0.13 ± 0.15	4	9.27 ± 0.26	9.30 ± 0.14	-0.03	75.9 ± 4.14***	0.09 ± 0.29	3
<i>I360A</i>	9.13 ± 0.18	8.99 ± 0.08	0.14	83.3 ± 9.47	0.22 ± 0.20	4	8.79 ± 0.14	8.79 ± 0.29	0.00	82.8 ± 35.9	0.08 ± 0.37	3
<i>A361L</i>	9.10 ± 0.18	9.52 ± 0.15	-0.42	77.8 ± 6.34*	-0.31 ± 0.24	4	9.15 ± 0.13	8.62 ± 0.40	0.53	67.4 ± 12.4*	0.70 ± 0.43	4
<i>E362A</i>	9.10 ± 0.18	9.00 ± 0.07	0.10	98.0 ± 6.53	0.11 ± 0.19	4	9.22 ± 0.10	8.91 ± 0.10	0.21	241.7 ± 76.1	-0.07 ± 0.20	3
<i>E363A</i>	9.00 ± 0.08	8.87 ± 0.15	0.13	93.9 ± 13.5	0.16 ± 0.18	4	9.22 ± 0.10	8.99 ± 0.11	0.23	217.7 ± 72.3	-0.11 ± 0.21	3
<i>V364A</i>	9.00 ± 0.08	8.84 ± 0.13	0.16	84.3 ± 8.49								

TABLE 2—continued

	AM ₁ receptor					<i>n</i>	AM ₂ receptor					<i>n</i>
	WT pEC ₅₀	Mutant pEC ₅₀	ΔLog pEC ₅₀	<i>E</i> _{max} (%WT)	ΔLog(RA)		WT pEC ₅₀	Mutant pEC ₅₀	ΔLog pEC ₅₀	<i>E</i> _{max} (%WT)	ΔLog(RA)	
TM7												
Y365A	9.09 ± 0.11	8.83 ± 0.11	0.26	68.9 ± 6.54**	0.42 ± 0.16	4	9.02 ± 0.12	8.51 ± 0.33	0.51	65.2 ± 0.85**	0.70 ± 0.35	3
D366A	8.97 ± 0.08	8.76 ± 0.15	0.21	69.9 ± 15.7	0.37 ± 0.19	4	9.17 ± 0.11	9.19 ± 0.30	-0.02	105.7 ± 23.8	-0.04 ± 0.33	3
Y367A	9.16 ± 0.10	9.11 ± 0.03	0.04	70.0 ± 6.69	0.20 ± 0.11	3	9.28 ± 0.17	8.61 ± 0.16*	0.67	163.7 ± 32.8	0.46 ± 0.25	3
I368A	9.06 ± 0.12	9.06 ± 0.08	0.00	77.3 ± 12.6	0.11 ± 0.16	4	9.28 ± 0.17	9.39 ± 0.25	-0.11	251.1 ± 120	-0.51 ± 0.37	3
M369A	9.06 ± 0.12	9.06 ± 0.13	0.00	185.1 ± 28.0*	-0.27 ± 0.19	4	9.28 ± 0.17	8.82 ± 0.27	0.46	295.7 ± 103.1	-0.01 ± 0.35	3

^a No curve, cAMP response was too low for a concentration-response curve to be fitted (pEC₅₀ and Δlog pEC₅₀ are denoted as <6 and >2).

^b Different from 0, as assessed by multiple t tests with the false discovery rate set to 1%.

^c ΔLog(RA) values where only the AM₂ receptor was active.

TABLE 3

Pharmacological parameters for ¹²⁵I-AM(13–52) binding for WT or mutant AM receptors

Common-differential residues are *bold italic* and differential residues are *italics*. Maximum specific binding is total binding (¹²⁵I-AM_{13–52} bound in the absence of competing ligand) minus the non-specific binding (¹²⁵I-AM_{13–52} bound in the presence of 3 μM AM).

	AM ₁ receptor			AM ₂ receptor		
	pIC ₅₀	Maximum specific binding (%WT)	<i>n</i>	pIC ₅₀	Maximum specific binding (%WT)	<i>n</i>
WT	8.56 ± 0.04		4	8.64 ± 0.07		4
<i>C212A</i>	8.06 ± 0.16	71.7 ± 20.7	3	8.35 ± 0.18	145.5 ± 23.4	3
<i>Y277A</i>	8.46 ± 0.35	34.3 ± 11.1 ^a	3	8.52 ± 0.15	97.4 ± 21.6	3
<i>C282A</i>	8.40 ± 0.15	85.4 ± 24.9	3	8.31 ± 0.29	180.4 ± 46.6	3
<i>I352A</i>	8.56 ± 0.10	43.5 ± 7.0 ^a	3	8.65 ± 0.21	42.2 ± 13.2 ^a	3

^a 95% confidence interval does not include 100%.

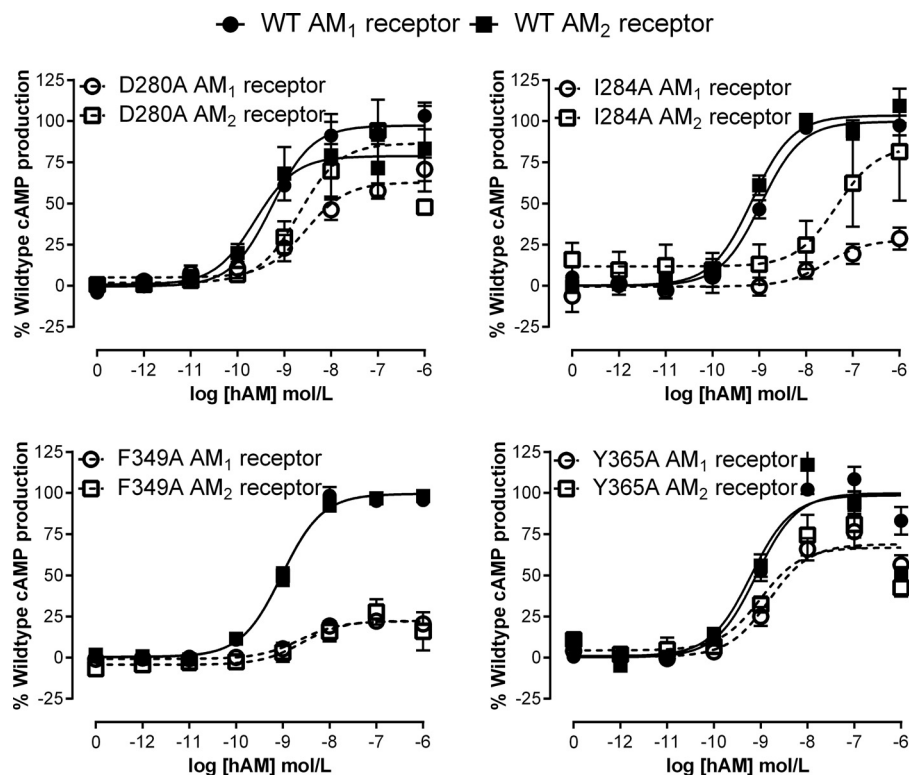


FIGURE 4. Examples of mutants with common effects on cAMP production in both the AM₁ and AM₂ receptors. Concentration-response curves are combined normalized data ± S.E. (error bars) for at least three individual experiments.

the residues with common cAMP effects are located in this invariant region and may contact the peptide (Fig. 9A). Residues with common but differential effects at each receptor also have largely similar orientations within the models (Fig. 9B). These residues are also mostly situated at the tops of the TM2 (Leu¹⁹⁵ and Val¹⁹⁸), TM3 (Cys²¹² and Lys²¹³), and TM6 (Ile³⁵², Pro³⁵³, and Trp³⁵⁴). Along with the common residues Ala¹⁹⁹ and Phe³⁴⁹ and common but differential Arg²⁷⁴, these form a network around the top of the TM helices. Differential residues

Tyr²⁷⁷ and Cys²⁸² are situated in ECL2 (Fig. 9C). Cys²¹², Tyr²⁷⁸, Cys²⁸², and Lys²¹³ do not appear to change their orientation significantly between the two AM receptors (Fig. 9, B and C). Lys²¹³ remains parallel to the Cys²¹²–Cys²⁸² bond, facing Tyr²⁷⁸ in both structures. Tyr²⁷⁷ moves outward in the AM₂ receptor and points away from the peptide binding pocket, thus changing its environment (Fig. 9C).

The most striking conformational difference between the AM₁ and AM₂ receptor models is the dramatic change in the

RAMP Effects on Adrenomedullin Receptors

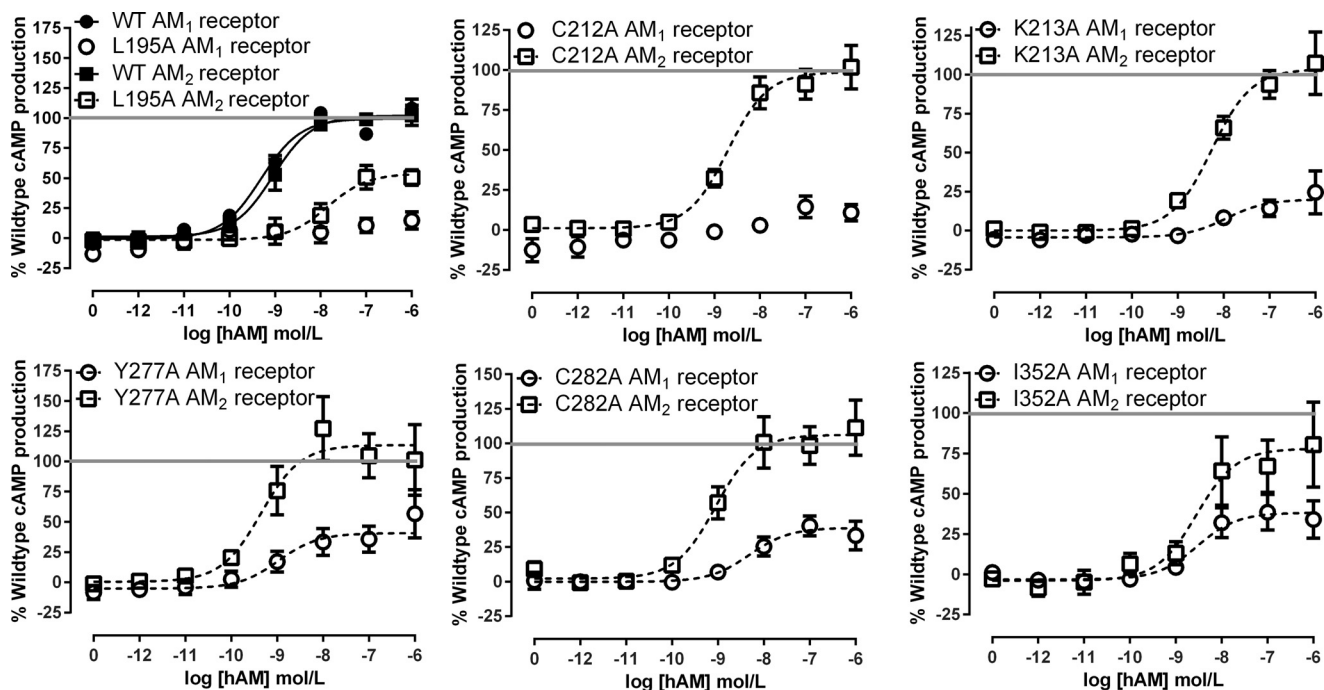


FIGURE 5. Examples of mutants with common-differential and differential (C282A and Y277A) effects on cAMP production between the AM receptors. WT curves were included in every experiment but are only shown as examples for L195A so that mutant differences between the receptors are not obscured by these curves in the other panels. The horizontal line represents maximal (100%) cAMP accumulation for the WT receptors. Concentration-response curves are combined normalized data \pm S.E. (error bars) for at least three individual experiments.

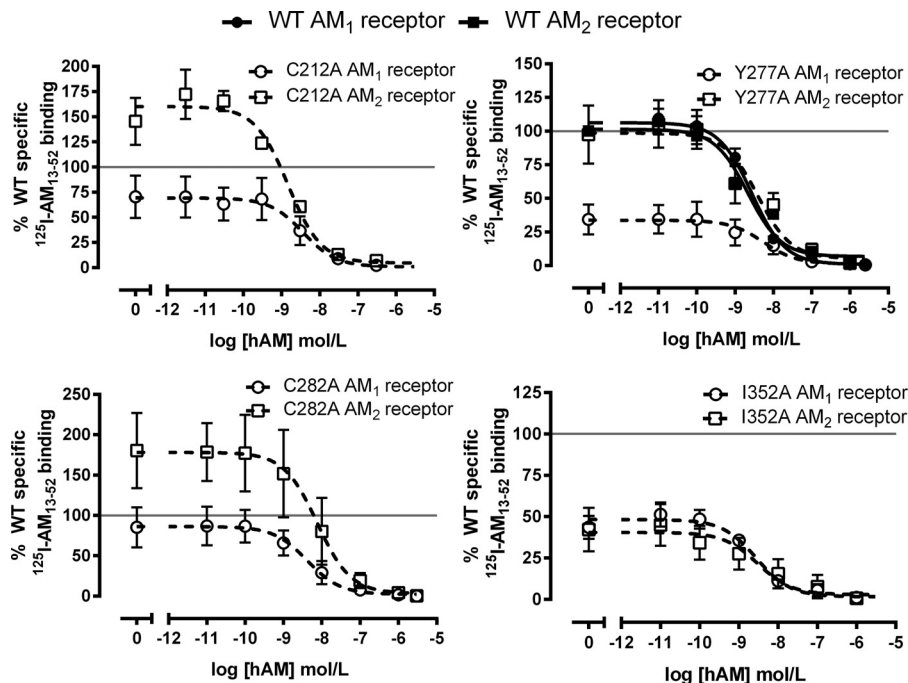


FIGURE 6. ^{125}I -AM(13-52) binding at selected mutants with common-differential and differential (Y277A and C282A) effects in cAMP assays. The curves are combined normalized data \pm S.E. (error bars) for three individual experiments.

position of ECL3 (Fig. 9D). The extracellular end of TM6 forms a distorted helix as a result of the influence of Pro³⁵³, Pro³⁵⁶, and Gly³⁵⁸. The conformation of ECL3 begins to diverge between the two models after the common differential residue Pro³⁵³. Trp³⁵⁴ stacks with ECL3 in the AM₁ receptor, whereas in the AM₂ receptor it is rotated by 90°, moving it away from the loop to face the lipid membrane. In the AM₂ receptor model,

ECL3 makes extensive contacts with AM, whereas in the AM₁ receptor, these contacts are minimal. The cumulative result of these differences is that distances relevant to the binding site vary in size (Fig. 9, E and F).

Probing the Model; Differential Peptide Contacts within the AM₁ and AM₂ Receptor TM Pockets—The divergence between the models translates into different transmembrane AM bind-

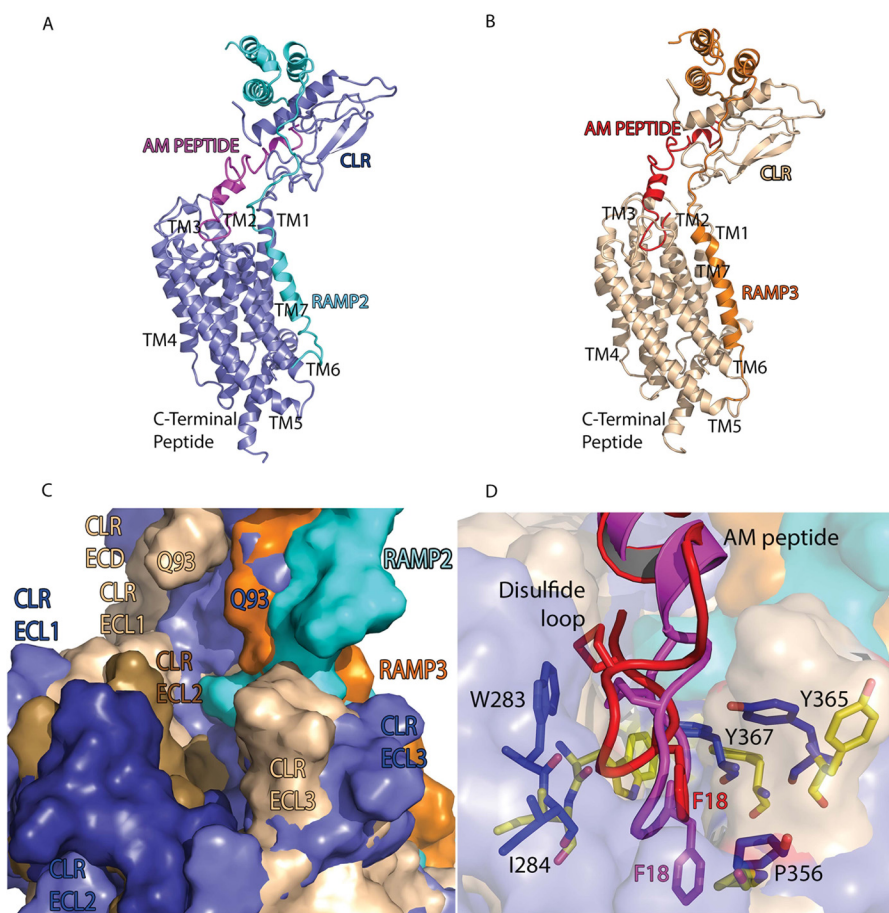


FIGURE 7. **Models of the full-length AM receptors.** *A*, AM₁ receptor; *B*, AM₂ receptor. Images were generated from an overlay aligning CLR residues 138–394 for both models (root mean square deviation = 2.0 Å). Relative sizes and orientations are thus not an artifact of figure generation. *C*, surface representation of the peptide binding pocket of the AM₁ and AM₂ receptors illustrating the changes in receptor conformation and the peptide binding pocket. *D*, close-up surface representation of the peptide binding pocket showing the docked AM peptide and its five close receptor neighbors, determined by the models in blue sticks (AM₁ receptor) and yellow sticks (AM₂ receptor). Other colors in *C* and *D* are as described for *A* and *B*.

ing pocket hull volumes of 4874 Å³ for the AM₁ receptor versus 3313 Å³ for the AM₂ receptor; the shapes of the two pockets also differ. The disulfide loop (Cys¹⁶–Cys²¹) of the docked AM peptide is located in the wide mouth of the peptide binding pocket with the side chain of Phe¹⁸ occupying the lower part of the pocket (Fig. 7*D*). Visual analysis and loop modeling indicated that Phe¹⁸, unlike its neighbors, occupied a more constrained pocket in the AM₂ receptor than in the AM₁ receptor. Consequently, we examined R17A, F18A, G19A, and T20A mutations in both the AM₁ and AM₂ receptors using MODELER; 100 models were generated, and the model with the best DOPE score was analyzed. In each case, apart from F18A, there was an equivalent decrease in the number of contacts (<4 Å) in both AM₁ and AM₂, but for F18A, there was a bigger decrease in the number of side chain contacts in the AM₁ receptor (from eight to two) rather than in the AM₂ receptor (from six to two). We therefore proposed that substitution of Phe¹⁸ with alanine would have a greater impact in the AM₁ receptor, compared with the AM₂ receptor. Consistent with our hypothesis, an F18A AM peptide stimulated cAMP production to a lesser degree at the AM₁ receptor (60% decrease in E_{\max}) than at the AM₂ receptor (no change in E_{\max}) (Table 4 and Fig. 10). This demonstrates that it is possible to engineer ligand-specific effects at these two receptors.

Small Molecule Druggability of the AM Receptors—We next analyzed the two receptor binding pockets for their druggability for small molecule, orally bioavailable ligands using the PockDrug and DoGSiteScorer druggability servers (52–54), which were trained to predict pockets with promising properties for the design of small molecule druglike ligands. Because druggability analysis is highly dependent on the cavity detection (53), we only discuss residues predicted by both servers to reside in the main helical binding pocket, namely 43 residues common to the AM₁ receptor pocket and 31 for the smaller AM₂ receptor pocket; these consensus residues largely coincide with the largest subpocket given by DoGSiteScorer. This analysis showed that the main druggable pocket in the helical domain of each AM receptor partially overlapped with the peptide binding pocket identified by our models (Fig. 11, *A* and *B*). In both receptors, the druggable pocket includes the hydrophobic patch at the top of TM2 (e.g. Leu¹⁹⁵), the distal residues of ECL2 (Trp²⁸³–Thr²⁸⁸), and residues on TM3 (e.g. Asp³⁶⁶, Tyr³⁶⁷, and His³⁷⁰). The druggable pockets extend below the limits of the peptide binding pocket and include Met²²³ and Tyr²²⁷ on TM3 for both receptors, but the AM₁ pocket includes other TM3 residues (e.g. Leu²²⁰). The druggable pockets also extend lower on TM6 to include Ile³⁷⁰ and Ile³⁷¹ for the AM₁ receptor. The AM₁ pocket includes more residues on TM1 (e.g.

RAMP Effects on Adrenomedullin Receptors

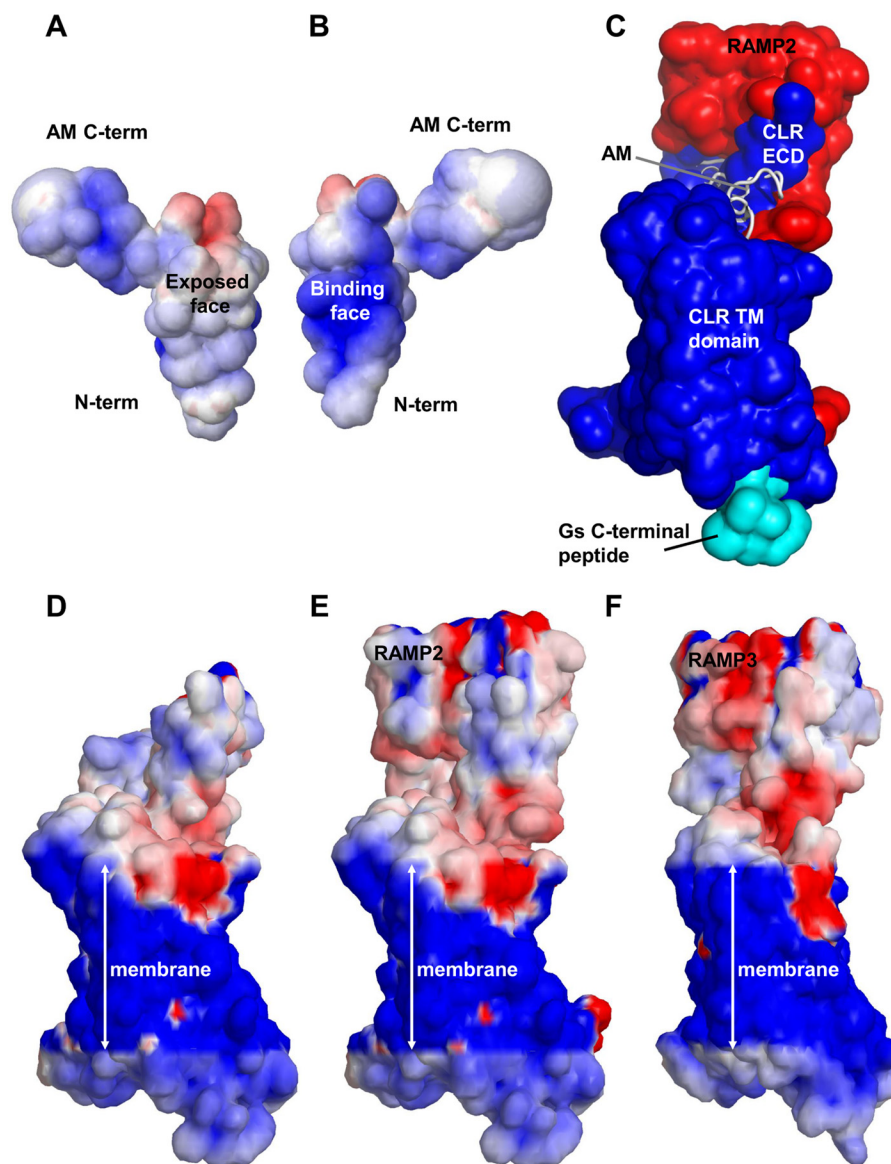


FIGURE 8. The electrostatic potential of AM, CLR, and the AM₁ and AM₂ receptors. *Blue*, positive; *red*, negative; the potential has been contoured between -5 and $+5$ onto the solvent-accessible surface. *A*, the electrostatic potential on the face of AM that is exposed as it binds to the CLR ECD; the electrostatic potential is weakly positive, and the general orientation is as shown in *C*. *B*, the electrostatic potential on the ECD-binding surface, as defined by *C*; the electrostatic potential is strongly positive. The $+4$ charge on AM includes the N-terminal amine. *C*, a representation of AM binding to the AM₁ receptor that can be used to identify the peptide-binding region in *D–F*: the CLR solvent-accessible surface is *blue*, the RAMP surface is *red*, and the C-terminal peptide of G_s is *cyan*. The solvent radius was expanded to 2.4 Å to mimic that in *D–F*. AM is shown in *white*. *D*, CLR electrostatic potential. *E*, AM₁ electrostatic potential. *F*, AM₂ electrostatic potential. The electrostatic potential of the AM₁ and AM₂ receptors was evaluated in an implicit membrane using APBS (the Adaptive Poisson-Boltzmann Solver) coupled with apbs_mem version 2.0 and the pdb2PQR server (74–76). The parameters for the APBSmem calculations were as follows: PARSE atomic charges (77); temperature, 298.15 K; ionic strength, 0.15 mM; protein and membrane relative dielectric constant, 2.0; relative solvent dielectric, 80; membrane thickness, 40 Å. The grid lengths were 300 × 300 × 300 Å with two levels of focusing; the grid dimensions were 97 × 97 × 97 for *A* and *B* and 129 × 129 × 225 for *D–F*. The CHARMM-gui was used to assist in placing the receptor within the membrane (78).

Thr¹⁴⁵ and His¹⁴⁹). Twenty-four residues were unique to the AM₁ receptor, and seven were unique to the AM₂ receptor, indicating that selectivity is possible. Some of the residues listed as part of the druggable pocket are more accessible than others (e.g. Phe²²⁸ in the AM₁ receptor is not obviously accessible in the absence of induced fit, because it is partially shielded by Tyr²²⁷), but such residues may nevertheless be important in drug design. The AM₁ receptor pocket reaches 14 Å below the top of ECL3 with drug scores of 0.97 and 0.81, from PockDrug and DoGSiteScorer, respectively. The AM₂ receptor drug-gable pocket forms a narrow channel and is deeper (partly

because of the ECL3 conformation), with PockDrug and DoGSiteScorer drug scores of 0.91 and 0.81, respectively; because the scores are above 0.5, both receptors are predicted to be druggable.

Discussion

Pharmacological tools to help tease out the relative importance of each of the two AM receptors are needed, but it has not been apparent how to develop these because both receptors share the common GPCR, CLR. We report that RAMP2 and RAMP3 confer conformational variation in the CLR juxtamem-

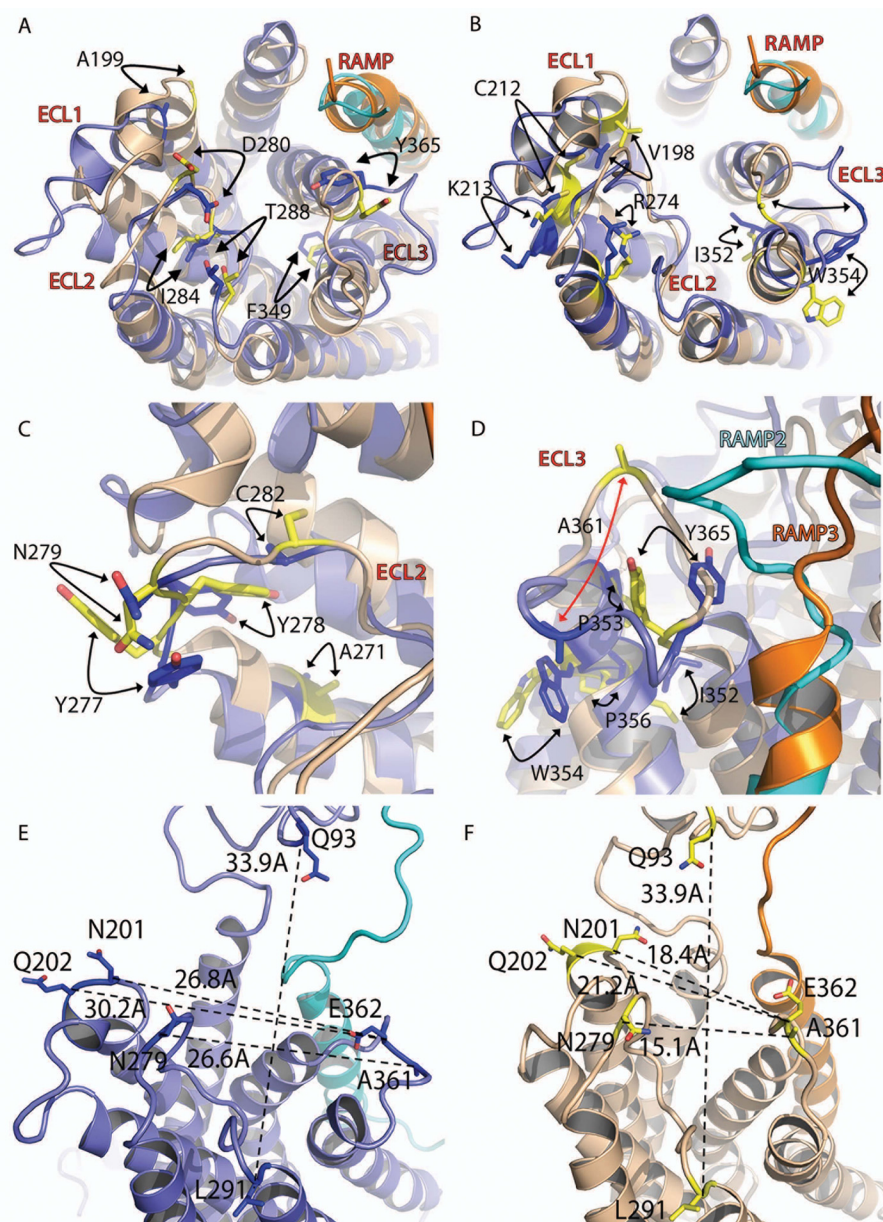


FIGURE 9. **Receptor model overlay.** Residues with common (A), common-differential (B), or differential (C) effects are shown as sticks, with oxygen atoms in red and nitrogen in blue. A, residues Ala¹⁹⁹, Asp²⁸⁰, Ile²⁸⁴, and Phe³⁴⁹ have similar side chain and main chain orientations; Tyr³⁶⁵ has side chain rotation of $\sim 180^\circ$ between the two AM receptors. B, residues Lys²¹³, Ile³⁵², and Trp³⁵⁴ have similar main chain but differing side chain orientations. C, Tyr²⁷⁷ shows substantial movement between the two receptors, whereas Tyr²⁷⁸ shows some movement but maintains similar interactions. D, close-up view of TM6-ECL3-TM7 showing the main residues involved in the change of the ECL3 position (red arrow denotes change in position). The increased proximity of RAMP2 to the CLR ECL3 in the AM₁ receptor is clearly visible. AM₁ and AM₂ receptors are colored as per the figure; the movement of residues between the receptors is shown with arrows. E and F, juxtamembrane region of the two receptors with distances between residues (dotted lines) in Å. Distances were measured between the same set of C α atoms in both receptors.

TABLE 4

Pharmacological parameters of cAMP accumulation for F18A substituted AM(15–52) versus wild type (WT) AM(15–52) stimulation of the WT AM₁ and AM₂ receptors

*, $p < 0.05$; ***, $p < 0.001$. Data analyzed by unpaired t test versus WT.

	WT AM(15–52) pEC ₅₀	F18A AM(15–52) pEC ₅₀	Δ Log EC ₅₀	% E_{\max} WT AM(15–52)	n
AM ₁ receptor	8.89 \pm 0.13	7.85 \pm 0.11***	1.04	40.3 \pm 9.73***	4
AM ₂ receptor	8.91 \pm 0.24	7.42 \pm 0.24*	1.49	101.7 \pm 5.26	3

brane region, yielding distinct binding pockets that may be tractable for the development of selective pharmacological tools and future drugs.

Our study combined extensive mutagenesis of CLR with independent modeling studies (*i.e.* not adjusted to enhance agreement with data tables) that allowed us to effectively interpret

RAMP Effects on Adrenomedullin Receptors

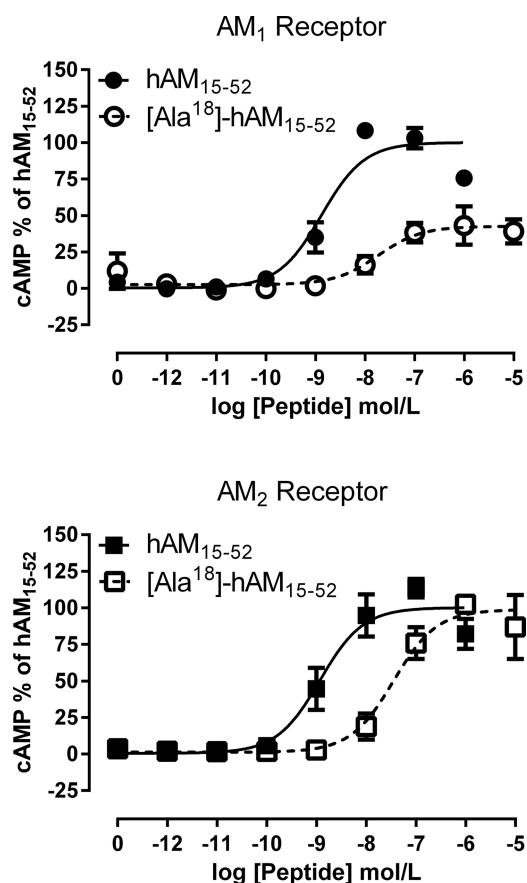


FIGURE 10. Concentration-response curves for the alanine-substituted AM peptide, F18A AM(15–52). Curves are combined normalized data from at least three individual experiments \pm S.E. (error bars).

our complex data set. Recent crystallographic and modeling studies have generated a consensus conformation for the TM bundle of the class B GPCRs (26, 43, 50, 55). Crystallographic studies have so far, however, proved unsatisfactory for determining the structure for a complete class B GPCR or for the class B ECL conformation due to the inherent mobility of the loops. The only structural data on the arrangement of the ECD of a class B GPCR with respect to the TM bundle comes from an electron microscopy study of the GCGR, and this is necessarily low resolution (56). Although molecular models do not have the accuracy of x-ray structures, they are nevertheless useful for providing a framework against which experimental results can be considered. While it would be unwise to overinterpret any model, ours is largely consistent with the effects of the mutagenesis (Table 5) and also successfully predicted the activity of F18A AM.

We initially compare our AM receptor models with that of the GCGR model structure (43), a canonical class B GPCR that does not require a RAMP. The main difference in the receptor is a $\sim 30^\circ$ change in the orientation of the ECD to a more open conformation as a result of the constraint created by the RAMP on the structure of the AM receptor. The orientation of the ECD is more consistent with the open (*i.e.* active, agonist-bound) conformational ensemble of the GCGR (56) than the closed ensemble because the difference between the centers of mass of the TM and ECD domains is $\sim 57 \text{ \AA}$, the polar angle θ is

similarly $\sim 23^\circ$, and the projection of the ECD center of mass onto the membrane plane lies outside of the helical bundle. In the GCGR, the simulated closed state described by Yang *et al.* (56) may well be the inactive conformation, satisfying the proposed ECD-ECL3 interaction proposed by Koth *et al.* (57), but in the AM receptors, because the RAMP binds to the peptide-binding face of the ECD, it is likely to inhibit formation of the fully closed conformation. The peptide shows more marked differences: the glucagon model peptide adopts a helical structure from Ser⁸ through to Met²⁷, spanning from the juxtamembrane region through to the ECD, in agreement with most x-ray crystal structures on isolated class B ECDs. In contrast, AM has a more complex structure, with a non-helical ECD region, in agreement with the x-ray crystal structure of the isolated ECD and a helical region that binds to the juxtamembrane region, as in previous related models and the AM NMR structure (40). The AM peptide helix binds to the same depth as the glucagon peptide, as judged by the alignment of the helical region (Fig. 1A), but the glucagon peptide N terminus binds to a greater depth (consistent with cross-linking data on the related PTH system (58), whereas AM forms a disulfide-bonded loop consistent not only with the binding of the usual AM(16–52) (26) but also AM(1–52) (*i.e.* the N terminus is orientated so that AM(1–15) can “escape” from the TM bundle). This N-terminal extension of AM does not seem important for AM activity, and the AM(15–52) fragment is more consistent with the length of other peptides in the AM family.

We have pharmacological evidence of RAMP-induced changes in the function of CLR at the AM₁ and AM₂ receptors, which are reflected in conformational differences between our full-length AM₁ and AM₂ receptor models. The most striking difference between the two models is the ECL3 conformation; interestingly, this is a region that also shows large differences between the GCGR and CRF1R x-ray crystal structures. Although only Ala³⁶¹ in ECL3 shows any kind of differential activity, the residues flanking ECL3 do show this. Moreover, at the CGRP receptor, the CLR-RAMP1 complex, Ile³⁶⁰ is involved in receptor activation as opposed to Ala³⁶¹ in the AM receptors (24), giving additional evidence of differential activity in ECL3. The extracellular region of TM6 in the AM receptors does contain residues with common-differential activity, namely Ile³⁵², Pro³⁵³, and Trp³⁵⁴. The predicted stacking of Trp³⁵⁴ with ECL3 in the AM₁ receptor combined with changes in the positions of Ile³⁵² and Pro³⁵³ may stabilize the altered orientation of ECL3. In the AM₂ receptor, Trp³⁵⁴ lies perpendicular to its AM₁ receptor position, allowing ECL3 to lie further toward the center of the peptide binding pocket. Movement of the upper regions of TM3, TM6, and TM7 is involved in activation of class A GPCRs (59). Some of the differences observed between the two AM receptors could therefore be reflected in differential activity of residues in ECL3/TM7 (Ala³⁶¹ and Tyr³⁶⁷) and TM3 (Cys²¹² and Lys²¹³) in the two AM receptors and in the CGRP receptor, where Cys²¹² is the only one of these residues involved in receptor activation (24).

The AM model peptide interacts differently with ECL3/TM7 in the two AM receptors (Figs. 1 and 7, A and B) in response to the effect of the different RAMPs; our models place the RAMP TM helix between TM6 and TM7 as in the class B secretin

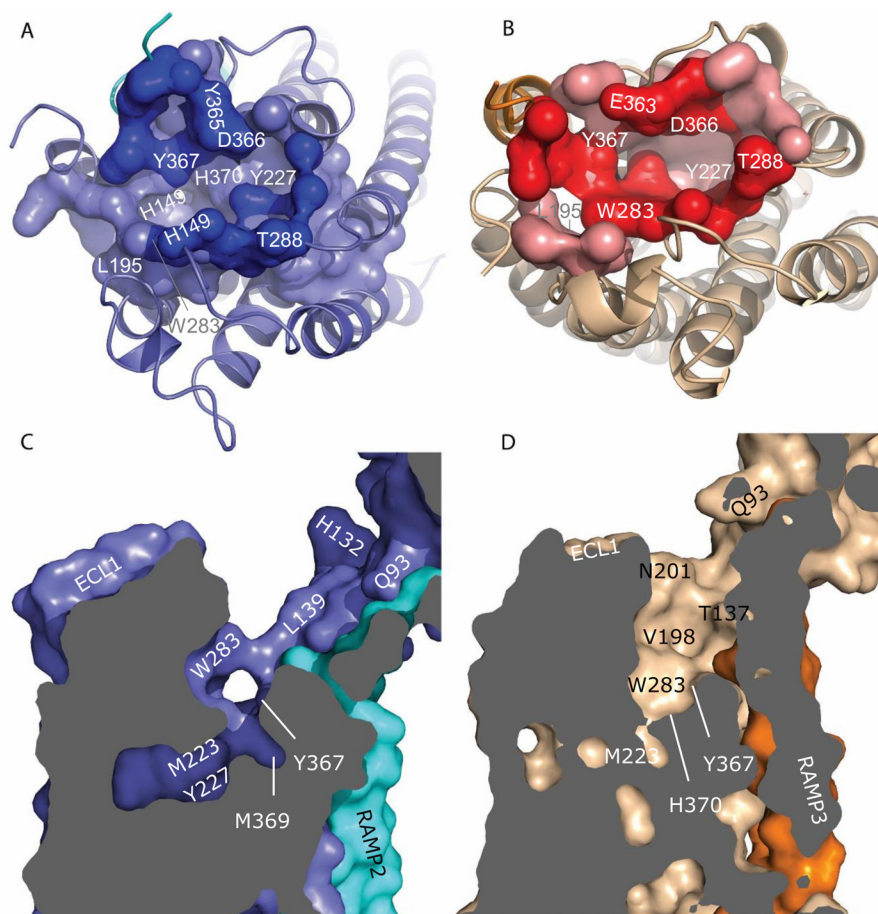


FIGURE 11. **Small molecule druggable sites predicted using PockDrug and viewed from above.** *A*, the AM₁ site is shown in *light blue*, and the site residues that contact AM are shown in *blue*. *B*, the AM₂ site is shown in *magenta*, and the site residues that contact AM are shown in *red*. This site is narrower and deeper than the AM₁ site; the PockDrug druggability scores for the AM₁ and AM₂ sites are 0.97 and 0.91, respectively. *C* and *D*, surface cutaway views of the receptors; the different size, conformation, and situation of the pockets are evident from the *shading*. Selected residues are *labeled*.

receptor (60). The greater proximity of the RAMP2 ECD-TM linker to ECL3 is probably the main factor that contributes to the reorientation of ECL3 (Fig. 9D). RAMP2 and RAMP3 diverge in sequence in this region, and equivalent RAMP residues take up different positions relative to AM in the two models.

The majority of the residues with a common or a common but differential effect on receptor activation vary little in their orientation and cluster around the upper TMs of our models (e.g. the hydrophobic cluster at the top of TM2 (Leu¹⁹⁵, Val¹⁹⁸, and Ala¹⁹⁹), which is also essential to the function of the CGRP receptor (24). There are also common and common-differential residues situated in ECL2 (Asp²⁸⁰, Trp²⁸³, and Ile²⁸⁴); due to the position of the disulfide bond in our AM receptor models, these lie in close proximity to the upper TMs. Indeed, many of these common and common-differential residues are also essential for the activation of the CGRP receptor by both CGRP and AM (26). ECL2 is particularly important in activation in class A and B GPCRs (26, 59, 61).

Cys²⁸² in ECL2 forms an essential conserved disulfide bond with Cys²¹² in TM3 in both the AM receptors and in the CGRP receptor (26). However, this bond does not appear to be critical to activation of the AM₂ receptor (or the CGRP receptor). The smaller pocket in the AM₂ receptor causes tighter packing

of the common and common-differential residue network around the top of the TMs; this more restrained environment may limit the movement of the side chain of either Cys²¹² or Cys²⁸² and allow the AM₂ receptor to tolerate an unpaired cysteine residue without detrimental perturbation of its structural integrity and thus activation of the AM₂ receptor. Significantly, ECL3 in the CGRP receptor adopts a similar conformation to the AM₂ receptor (results not shown). In the more open AM₁ receptor, this C212A or C282A mutation is fatal to receptor activation, but precise verification of the mechanism is beyond the scope of our models. However, we propose that the greater effect of mutation at the common but differential residues in the AM₁ receptor is related to its degree of openness and hence stability. Thus, we note that other residues, such as Lys²¹³, Tyr²⁷⁷, and Tyr²⁷⁸, that are predicted to stabilize ECL2 also show more pronounced effects on mutation in the AM₁ receptor despite generally adopting similar interactions (Lys²¹³ and Tyr²⁷⁸) in both structures, presumably because the mutated AM₁ receptor structure is less stable than the mutated AM₂ structure.

These changes, especially those in ECL3, serve to alter the depth, volume, shape, and composition of the model binding pocket. Whereas the overall position of the docked peptide and in particular the Phe¹⁸ side chain in the peptide binding pocket

RAMP Effects on Adrenomedullin Receptors

TABLE 5

Comments on the mutation data of residues discussed in this work and shown in Tables 1 and 2 in light of the receptor models

Common residues are shown in boldface type, common-differential residues are in boldface italic type, and differential residues are in italic type.

	Residue	Comments	AM ₁ Receptor	AM ₂ Receptor
TM2	L195	L195 essential for ligand binding (similar in glucagon receptor). All 3 form a hydrophobic patch. The residues support ECL2 in the region of W283	No response to AM	Decreased E _{max} and EC ₅₀
	V198		Decreased EC ₅₀	Decreased EC ₅₀ , increased E _{max}
	A199		Decreased E _{max} and EC ₅₀	Decreased EC ₅₀
TM3	C212	Disulfide. Essential in AM ₁ , smaller effect in AM ₂ receptor	No response to AM	Decreased EC ₅₀
	K213	Possibly a charged residue at lipid-water interface that defines top of TM3 and helps to anchor it. Helps to stabilize the conformation of the N-terminal part of ECL2 (as in the glucagon receptor structure). Essential for AM ₁ ; mutation less severe for AM ₂ .	Decreased E _{max} and EC ₅₀	Decreased EC ₅₀
TM4	A271	Adjacent to F217 and L220 of TM2; structural role in stabilizing ECL2?	Decreased E _{max} and EC ₅₀	No Effect
	R274	Conserved as Arg or Lys; faces ECL2 in CRFR1 structure 4K5Y. Structural role in shaping N-terminal part of ECL2. Also close to G19 of AM. Very strong effect in AM ₁ , strong, but less so in AM ₂ receptor.	Decreased E _{max} and EC ₅₀	Decreased E _{max} and EC ₅₀
ECL2	Y277	Buttresses ECL2; close to ring of AM in AM ₁ . No contacts in AM ₂ as faces out.	Decreased E _{max} and EC ₅₀	No Effect
	Y278	Buttresses ECL2; contacts K213 in AM ₁ and AM ₂ but probably has a larger effect in more open AM ₁ . Y277, Y278 do not contact other aromatics	Decreased E _{max} and EC ₅₀	No Effect
	N279	Faces Q24 of AM in AM ₁ . No contacts in AM ₂ as faces out	Decreased E _{max} and EC ₅₀	No Effect
	D280	Close to T20 of AM in AM ₁ and backbone of L26 in AM ₂	Decreased E _{max} and EC ₅₀	Decreased EC ₅₀
	C282	Disulphide	Decreased E _{max} and EC ₅₀	No effect
	W283	Major contact at base of AM binding pocket. Also structural. Contacts base of AM and TM2. Proximity of the equivalent of this residue in the GLP-1R to I30 of GLP-1 in cross-linking studies on GLP-1R (79) is consistent with models	Decreased E _{max} and EC ₅₀	Decreased EC ₅₀
	I284	Buttresses ECL2; structural. Contacts, ECL2 and TM3	Decreased E _{max} and EC ₅₀	Decreased E _{max} and EC ₅₀
	T288	A contact of T20	Decreased E _{max} and EC ₅₀	Decreased EC ₅₀
	TM6	F349	Inward facing, very deep, maintain binding pocket in both AM ₁ and AM ₂ receptor	Decreased E _{max}
L351		Outward facing	Aberrant expression	Aberrant expression
I352		As F349 – the TM6 residues F349-W354 form a hydrophobic cluster, but closer to F18 of AM in AM ₂ than in AM ₁ receptor	Decreased E _{max} and EC ₅₀	Decreased E _{max}
P353		Base of binding pocket in both AM ₁ and AM ₂ receptor. Different overall ECL3 positions may explain differential roles. Close to AM in AM ₂ .	No response to AM	Decreased E _{max} and EC ₅₀
W354		Possibly stabilises the marked backward bend in ECL3. This is seen with AM ₁ but not AM ₂ receptor, consistent with the subtype selectivity	Decreased E _{max} and EC ₅₀	Decreased EC ₅₀
ECL3	E357	Contact with Y292/H295 in TM6; polar residue at lipid-water interface	Aberrant expression	Aberrant expression
	A361	Weak contact of V23/K25 of AM at AM ₂ (but not AM ₁). Effect may be related to small size.	Decreased E _{max} and ΔLog(RA)	Decreased E _{max} , increased ΔLog(RA)
	Y365	AM ₁ receptor: Contacts to R17, T22 of AM. AM ₂ receptor: faces out, possibly involved in stabilizing ECL3 conformation	Decreased E _{max}	Decreased E _{max}
TM7	Y367	Contact R17 of AM, TM1 and top of RAMP TM		Decreased EC ₅₀

does not change significantly, the number of close neighbors to the Phe¹⁸ side chain does. These changes have significant implications for the design of therapeutics that are either specific to the AM₁ or AM₂ receptors to treat receptor-specific pathophysiology or conversely to harness the common effects of both receptors. Druggability screening highlighted two different druggable pockets for small molecules in the AM₁ and AM₂ receptors. This indicates scope for specific ligand design by tar-

getting the additional and differential druggable residues of the two pockets, which lie within the TM domains.

The drug scores of 0.81–0.97 and 0.81–0.91 for the AM₁ and AM₂ receptors, respectively, are clearly above the 0.5 threshold, indicating that they are druggable. Significantly, both sites display an appropriate balance of hydrophobic and polar residues, as required for a druggable site (62). Moreover, the difference in electrostatic potential for these receptors adds to the rationale for the design of selective AM₁ or AM₂ ligands. In addition, the structural model of the AM peptide structure (Fig. 1E) is distinctly different from that of glucagon and probably many other class B peptide ligands and so may also be useful in substrate-based drug design, especially because there are differences in the two loop regions. The CRF1R structure shows a narrow drug-bound channel that sits below the level of our peptide binding site. Interestingly, both druggability servers indicate additional druggable sites in this region (20).

We have based our current study on the measurement of cAMP as the canonical signaling pathway for CLR. It is important to note that GPCRs, such as this, also have the capacity to signal through alternative pathways, and it will be important to consider these in future studies (55). It is possible that some residues will have a greater or lesser role, depending on the pathway measured, indicating further conformational differences in the receptors.

In summary, we suggest that the change in the predicted conformation of ECL3 and hence the different TM binding pockets in the AM₁ and AM₂ receptors is due to association with different RAMPs, as described above. The existence of distinct peptide and small molecule binding pockets with different properties has implications for the design of selective therapeutics, whether they be small molecules or peptides. This could facilitate the design of ligands to harness the individual physiological roles of the two AM receptors, validating the receptors as drug targets.

Our data support the idea that RAMPs act allosterically to modify the conformation of CLR. This could lead to a range of possible outcomes, including biasing the receptor toward different ligands or signaling pathways. Two recent reports have suggested this mechanism for RAMP effects on the related calcitonin receptor (63, 64). Allostery between protomers in receptor oligomers could be a broad mechanism for generating diversity in GPCR function.

Author Contributions—H. A. W., J. J. G., M. C., R. S. A., and M. G. conducted experiments. C. A. R., M. P., J. M. W. R. M., A. L., and A. C. contributed to the modeling. P. W. R. H., T.-Y. Y., and M. A. B. were responsible for peptide synthesis. J. B., D. R. P., M. J. W., and A. C. C. contributed receptor mutants to the study. A. A. P. provided data that were used for the modeling. C. A. R., H. A. W., D. R. P., and D. L. H. interpreted the experiments and wrote the paper.

Acknowledgment—The GCGR-glucagon model (43) was kindly provided by Stevens and co-workers.

References

- Nishikimi, T., Kuwahara, K., Nakagawa, Y., Kangawa, K., and Nakao, K. (2013) Adrenomedullin in cardiovascular disease: a useful biomarker, its

- pathological roles and therapeutic application. *Curr. Protein Pept. Sci.* **14**, 256–267
2. Manuela, C., Laura, S., Benedetta, S., Raffaele, C., Alessandro, V., Chiara, C., Tommaso, P., Daniela, G., and Silvia, D. R. (2014) Adrenomedullin and intermedin gene transcription is increased in leukocytes of patients with chronic heart failure at different stages of the disease. *Peptides* **55**, 13–16
 3. Wong, C. P., Loh, S. Y., Loh, K. K., Ong, P. J., Foo, D., and Ho, H. H. (2012) Acute myocardial infarction: clinical features and outcomes in young adults in Singapore. *World J. Cardiol.* **4**, 206–210
 4. Burley, D. S., Hamid, S. A., and Baxter, G. F. (2007) Cardioprotective actions of peptide hormones in myocardial ischemia. *Heart Fail. Rev.* **12**, 279–291
 5. Nagaya, N., Nishikimi, T., Uematsu, M., Satoh, T., Oya, H., Kyotani, S., Sakamaki, F., Ueno, K., Nakanishi, N., Miyatake, K., and Kangawa, K. (2000) Haemodynamic and hormonal effects of adrenomedullin in patients with pulmonary hypertension. *Heart* **84**, 653–658
 6. Lainchbury, J. G., Nicholls, M. G., Espiner, E. A., Yandle, T. G., Lewis, L. K., and Richards, A. M. (1999) Bioactivity and interactions of adrenomedullin and brain natriuretic peptide in patients with heart failure. *Hypertension* **34**, 70–75
 7. Kataoka, Y., Miyazaki, S., Yasuda, S., Nagaya, N., Noguchi, T., Yamada, N., Morii, I., Kawamura, A., Doi, K., Miyatake, K., Tomoike, H., and Kangawa, K. (2010) The first clinical pilot study of intravenous adrenomedullin administration in patients with acute myocardial infarction. *J. Cardiovasc. Pharmacol.* **56**, 413–419
 8. Dupuis, J., Caron, A., and Ruël, N. (2005) Biodistribution, plasma kinetics and quantification of single-pass pulmonary clearance of adrenomedullin. *Clin. Sci.* **109**, 97–102
 9. Kato, J., and Kitamura, K. (2015) Bench-to bedside pharmacology of adrenomedullin. *Eur. J. Pharmacol.* **764**, 140–148
 10. Poyner, D. R., Sexton, P. M., Marshall, I., Smith, D. M., Quirion, R., Born, W., Muff, R., Fischer, J. A., and Foord, S. M. (2002) International Union of Pharmacology. XXXII. The mammalian calcitonin gene-related peptides, adrenomedullin, amylin, and calcitonin receptors. *Pharmacol. Rev.* **54**, 233–246
 11. Dackor, R. T., Fritz-Six, K., Dunworth, W. P., Gibbons, C. L., Smithies, O., and Caron, K. M. (2006) Hydrops fetalis, cardiovascular defects, and embryonic lethality in mice lacking the calcitonin receptor-like receptor gene. *Mol. Cell. Biol.* **26**, 2511–2518
 12. Dackor, R., Fritz-Six, K., Smithies, O., and Caron, K. (2007) Receptor activity-modifying proteins 2 and 3 have distinct physiological functions from embryogenesis to old age. *J. Biol. Chem.* **282**, 18094–18099
 13. Caron, K. M., and Smithies, O. (2001) Extreme hydrops fetalis and cardiovascular abnormalities in mice lacking a functional adrenomedullin gene. *Proc. Natl. Acad. Sci. U.S.A.* **98**, 615–619
 14. Yoshizawa, T., Sakurai, T., Kamiyoshi, A., Ichikawa-Shindo, Y., Kawate, H., Iesato, Y., Koyama, T., Uetake, R., Yang, L., Yamauchi, A., Tanaka, M., Toriyama, Y., Igarashi, K., Nakada, T., Kashiwara, T., et al. (2013) Novel regulation of cardiac metabolism and homeostasis by the adrenomedullin-receptor activity-modifying protein 2 system. *Hypertension* **61**, 341–351
 15. Liang, L., Tam, C. W., Pozsgai, G., Siow, R., Clark, N., Keeble, J., Husmann, K., Born, W., Fischer, J. A., Poston, R., Shah, A., and Brain, S. D. (2009) Protection of angiotensin II-induced vascular hypertrophy in vascular smooth muscle-targeted receptor activity-modifying protein 2 transgenic mice. *Hypertension* **54**, 1254–1261
 16. Barrick, C. J., Lenhart, P. M., Dackor, R. T., Nagle, E., and Caron, K. M. (2012) Loss of receptor activity-modifying protein 3 exacerbates cardiac hypertrophy and transition to heart failure in a sex-dependent manner. *J. Mol. Cell. Cardiol.* **52**, 165–174
 17. Yamauchi, A., Sakurai, T., Kamiyoshi, A., Ichikawa-Shindo, Y., Kawate, H., Igarashi, K., Toriyama, Y., Tanaka, M., Liu, T., Xian, X., Imai, A., Zhai, L., Owa, S., Arai, T., and Shindo, T. (2014) Functional differentiation of RAMP2 and RAMP3 in their regulation of the vascular system. *J. Mol. Cell. Cardiol.* **77**, 73–85
 18. Tadokoro, K., Nishikimi, T., Mori, Y., Wang, X., Akimoto, K., and Matsumoto, H. (2003) Altered gene expression of adrenomedullin and its receptor system and molecular forms of tissue adrenomedullin in left ventricular hypertrophy induced by malignant hypertension. *Regul. Pept.* **112**, 71–78
 19. Garland, S. L. (2013) Are GPCRs still a source of new targets? *J. Biomol. Screen.* **18**, 947–966
 20. Hollenstein, K., de Graaf, C., Bortolato, A., Wang, M. W., Marshall, F. H., and Stevens, R. C. (2014) Insights into the structure of class B GPCRs. *Trends Pharmacol. Sci.* **35**, 12–22
 21. Booe, J. M., Walker, C. S., Barwell, J., Kuteyi, G., Simms, J., Jamaluddin, M. A., Warner, M. L., Bill, R. M., Harris, P. W., Brimble, M. A., Poyner, D. R., Hay, D. L., and Pioszak, A. A. (2015) Structural basis for receptor activity-modifying protein-dependent selective peptide recognition by a G protein-coupled receptor. *Mol. Cell* **58**, 1040–1052
 22. Watkins, H. A., Walker, C. S., Ly, K. N., Bailey, R. J., Barwell, J., Poyner, D. R., and Hay, D. L. (2014) Receptor activity-modifying protein-dependent effects of mutations in the calcitonin receptor-like receptor: implications for adrenomedullin and calcitonin gene-related peptide pharmacology. *Br. J. Pharmacol.* **171**, 772–788
 23. Qi, T., Dong, M., Watkins, H. A., Wootten, D., Miller, L. J., and Hay, D. L. (2013) Receptor activity-modifying protein-dependent impairment of calcitonin receptor splice variant $\Delta(1-47)$ hCT (a) function. *Br. J. Pharmacol.* **168**, 644–657
 24. Barwell, J., Conner, A., and Poyner, D. R. (2011) Extracellular loops 1 and 3 and their associated transmembrane regions of the calcitonin receptor-like receptor are needed for CGRP receptor function. *Biochim. Biophys. Acta* **1813**, 1906–1916
 25. Qi, T., Christopoulos, G., Bailey, R. J., Christopoulos, A., Sexton, P. M., and Hay, D. L. (2008) Identification of N-terminal receptor activity-modifying protein residues important for calcitonin gene-related peptide, adrenomedullin, and amylin receptor function. *Mol. Pharmacol.* **74**, 1059–1071
 26. Woolley, M. J., Watkins, H. A., Taddese, B., Karakullukcu, Z. G., Barwell, J., Smith, K. J., Hay, D. L., Poyner, D. R., Reynolds, C. A., and Conner, A. C. (2013) The role of ECL2 in CGRP receptor activation: a combined modelling and experimental approach. *J. R. Soc. Interface* **10**, 20130589
 27. Bailey, R. J., and Hay, D. L. (2006) Pharmacology of the human CGRP1 receptor in Cos 7 cells. *Peptides* **27**, 1367–1375
 28. Harris, P. W. R., Yang, S. H., and Brimble, M. A. (2011) An improved procedure for the preparation of aminomethyl polystyrene resin and its use in solid phase (peptide) synthesis. *Tetrahedron Lett.* **52**, 6024–6026
 29. Harris, P. W. R., Williams, G. M., Shepherd, P., and Brimble, M. A. (2008) The synthesis of phosphopeptides using microwave-assisted solid phase peptide synthesis. *Int. J. Pept. Res. Ther.* **14**, 387–392
 30. Vohra, S., Taddese, B., Conner, A. C., Poyner, D. R., Hay, D. L., Barwell, J., Reeves, P. J., Upton, G. J., and Reynolds, C. A. (2013) Similarity between class A and class B G-protein-coupled receptors exemplified through calcitonin gene-related peptide receptor modelling and mutagenesis studies. *J. R. Soc. Interface* **10**, 20120846
 31. Gingell, J. J., Qi, T., Bailey, R. J., and Hay, D. L. (2010) A key role for tryptophan 84 in receptor activity-modifying protein 1 in the amylin 1 receptor. *Peptides* **31**, 1400–1404
 32. McLatchie, L. M., Fraser, N. J., Main, M. J., Wise, A., Brown, J., Thompson, N., Solari, R., Lee, M. G., and Foord, S. M. (1998) RAMPs regulate the transport and ligand specificity of the calcitonin-receptor-like receptor. *Nature* **393**, 333–339
 33. Bailey, R. J., and Hay, D. L. (2007) Agonist-dependent consequences of proline to alanine substitution in the transmembrane helices of the calcitonin receptor. *Br. J. Pharmacol.* **151**, 678–687
 34. Conner, A. C., Hay, D. L., Simms, J., Howitt, S. G., Schindler, M., Smith, D. M., Wheatley, M., and Poyner, D. R. (2005) A key role for transmembrane prolines in calcitonin receptor-like receptor agonist binding and signalling: implications for family B G-protein-coupled receptors. *Mol. Pharmacol.* **67**, 20–31
 35. Kenakin, T. P. (2014) *A Pharmacology Primer: Techniques for More Effective and Strategic Drug Discovery*, 4th Ed., pp. 181–211, Elsevier, Amsterdam
 36. Lock, A., Forfar, R., Weston, C., Bowsher, L., Upton, G. J. G., Reynolds, C. A., Ladds, G., and Dixon, A. M. (2014) One motif to bind them: a

RAMP Effects on Adrenomedullin Receptors

- small-XXX-small motif affects transmembrane domain 1 oligomerization, function, localization, and cross-talk between two yeast GPCRs. *Biochim. Biophys. Acta* **1838**, 3036–3051
37. Jacobson, M. P., Pincus, D. L., Rapp, C. S., Day, T. J., Honig, B., Shaw, D. E., and Friesner, R. A. (2004) A hierarchical approach to all-atom protein loop prediction. *Proteins* **55**, 351–367
 38. Watkins, H. A., Au, M., and Hay, D. L. (2012) The structure of secretin family GPCR peptide ligands: implications for receptor pharmacology and drug development. *Drug Discov. Today* **17**, 1006–1014
 39. Larkin, M. A., Blackshields, G., Brown, N. P., Chenna, R., McGettigan, P. A., McWilliam, H., Valentin, F., Wallace, I. M., Wilm, A., Lopez, R., Thompson, J. D., Gibson, T. J., and Higgins, D. G. (2007) Clustal W and Clustal X version 2.0. *Bioinformatics* **23**, 2947–2948
 40. Pérez-Castells, J., Martín-Santamaría, S., Nieto, L., Ramos, A., Martínez, A., Pascual-Teresa, B., and Jiménez-Barbero, J. (2012) Structure of micelle-bound adrenomedullin: a first step toward the analysis of its interactions with receptors and small molecules. *Biopolymers* **97**, 45–53
 41. Taddese, B., Upton, G. J. G., Bailey, G. R., Jordan, S. R. D., Abdulla, N. Y., Reeves, P. J., and Reynolds, C. A. (2014) Do plants contain G protein-coupled receptors? *Plant Physiol.* **164**, 287–307
 42. Runge, S., Thøgersen, H., Madsen, K., Lau, J., and Rudolph, R. (2008) Crystal structure of the ligand-bound glucagon-like peptide-1 receptor extracellular domain. *J. Biol. Chem.* **283**, 11340–11347
 43. Siu, F. Y., He, M., de Graaf, C., Han, G. W., Yang, D., Zhang, Z., Zhou, C., Xu, Q., Wacker, D., Joseph, J. S., Liu, W., Lau, J., Cherezov, V., Katritch, V., Wang, M. W., and Stevens, R. C. (2013) Structure of the human glucagon class B G-protein-coupled receptor. *Nature* **499**, 444–449
 44. Eswar, N., Webb, B., Marti-Renom, M. A., Madhusudhan, M. S., Eramian, D., Shen, M. Y., Pieper, U., and Salí, A. (2007) Comparative protein structure modeling using MODELLER. *Curr. Protoc. Protein Sci.* 10.1002/0471140864.ps0209s50
 45. Humphrey, W., Dalke, A., and Schulten, K. (1996) VMD: visual molecular dynamics. *J. Mol. Graphics* **14**, 33–38
 46. Colovos, C., and Yeates, T. O. (1993) Verification of protein structures: patterns of nonbonded atomic interactions. *Protein Sci.* **2**, 1511–1519
 47. Rasmussen, S. G. F., DeVree, B. T., Zou, Y. Z., Kruse, A. C., Chung, K. Y., Kobilka, T. S., Thian, F. S., Chae, P. S., Pardon, E., Calinski, D., Mathiesen, J. M., Shah, S. T. A., Lyons, J. A., Caffrey, M., Gellman, S. H., et al. (2011) Crystal structure of the β_2 adrenergic receptor-Gs protein complex. *Nature* **477**, 549–555
 48. Roy, A., Taddese, B., Vohra, S., Thimmaraju, P. K., Illingworth, C. J. R., Simpson, L. M., Mukherjee, K., Reynolds, C. A., and Chintapalli, S. V. (2014) Identifying subset errors in multiple sequence alignments. *J. Biomol. Struct. Dyn.* **32**, 364–371
 49. Baldwin, J. M., Schertler, G. F. X., and Unger, V. M. (1997) An α -carbon template for the transmembrane helices in the rhodopsin family of G-protein-coupled receptors. *J. Mol. Biol.* **272**, 144–164
 50. Hollenstein, K., Kean, J., Bortolato, A., Cheng, R. K., Doré, A. S., Jazayeri, A., Cooke, R. M., Weir, M., and Marshall, F. H. (2013) Structure of class B GPCR corticotropin-releasing factor receptor 1. *Nature* **499**, 438–443
 51. Wootten, D., Reynolds, C. A., Koole, C., Smith, K. J., Mobarec, J. C., Simms, J., Quon, T., Furness, S. G., Miller, L. J., Christopoulos, A., and Sexton, P. M. (2016) A hydrogen-bonded polar network in the core of the glucagon-like peptide-1 receptor is a fulcrum for biased agonism: lessons from class B crystal structures. *Mol. Pharmacol.* **89**, 335–347
 52. Hussein, H. A., Borrel, A., Geneix, C., Petitjean, M., Regad, L., and Camproux, A. C. (2015) PockDrug-Server: a new web server for predicting pocket druggability on holo and apo proteins. *Nucleic Acids Res.* **43**, W436–W442
 53. Borrel, A., Regad, L., Xhaard, H., Petitjean, M., and Camproux, A. C. (2015) Pock drug: a model for predicting pocket druggability that overcomes pocket estimation uncertainties. *J. Chem. Inf. Model.* **55**, 882–895
 54. Volkamer, A., Kuhn, D., Rippmann, F., and Rarey, M. (2012) DoGSite-Scorer: a web server for automatic binding site prediction, analysis and druggability assessment. *Bioinformatics* **28**, 2074–2075
 55. Wootten, D., Simms, J., Miller, L. J., Christopoulos, A., and Sexton, P. M. (2013) Polar transmembrane interactions drive formation of ligand-specific and signal pathway-biased family B G protein-coupled receptor conformations. *Proc. Natl. Acad. Sci. U.S.A.* **110**, 5211–5216
 56. Yang, L., Yang, D., de Graaf, C., Moeller, A., West, G. M., Dharmarajan, V., Wang, C., Siu, F. Y., Song, G., Reedtz-Runge, S., Pascal, B. D., Wu, B., Potter, C. S., Zhou, H., Griffin, P. R., et al. (2015) Conformational states of the full-length glucagon receptor. *Nat. Commun.* **6**, 7859
 57. Koth, C. M., Murray, J. M., Mukund, S., Madjidi, A., Minn, A., Clarke, H. J., Wong, T., Chiang, V., Luis, E., Estevez, A., Rondon, J., Zhang, Y., Hötzel, I., Allan, B. B. (2012) Molecular basis for negative regulation of the glucagon receptor. *Proc. Natl. Acad. Sci. U.S.A.* **109**, 14393–14398
 58. Monaghan, P., Thomas, B. E., Woznica, I., Wittelsberger, A., Mierke, D. F., and Rosenblatt, M. (2008) Mapping peptide hormone-receptor interactions using a disulfide-trapping approach. *Biochemistry* **47**, 5889–5895
 59. Wheatley, M., Wootten, D., Conner, M. T., Simms, J., Kendrick, R., Logan, R. T., Poyner, D. R., and Barwell, J. (2012) Lifting the lid on GPCRs: the role of extracellular loops. *Br. J. Pharmacol.* **165**, 1688–1703
 60. Harikumar, K. G., Simms, J., Christopoulos, G., Sexton, P. M., and Miller, L. J. (2009) Molecular basis of association of receptor activity-modifying protein 3 with the family B G protein-coupled secretin receptor. *Biochemistry* **48**, 11773–11785
 61. Koole, C., Wootten, D., Simms, J., Miller, L. J., Christopoulos, A., and Sexton, P. M. (2012) Second extracellular loop of human glucagon-like peptide-1 receptor (GLP-1R) has a critical role in GLP-1 peptide binding and receptor activation. *J. Biol. Chem.* **287**, 3642–3658
 62. Bortolato, A., Doré, A. S., Hollenstein, K., Tehan, B. G., Mason, J. S., and Marshall, F. H. (2014) Structure of class B GPCRs: new horizons for drug discovery. *Br. J. Pharmacol.* **171**, 3132–3145
 63. Gingell, J. J., Simms, J., Barwell, J., Poyner, D. R., Watkins, H. A., Pioszak, A. A., Sexton, P. M., and Hay, D. L. (2016) An allosteric role for receptor activity-modifying proteins in defining GPCR pharmacology. *Cell Discov.*, in press
 64. Lee S. M., Hay, D. L., and Pioszak, A. A. (2016) Calcitonin and amylin receptor peptide interaction mechanisms: insights into peptide-binding modes and allosteric modulation of the calcitonin receptor by receptor activity-modifying proteins. *J. Biol. Chem.* **291**, 8686–8700
 65. Schneidman-Duhovny, D., Inbar, Y., Nussinov, R., and Wolfson, H. J. (2005) PatchDock and SymmDock: servers for rigid and symmetric docking. *Nucleic Acids Res.* **33**, W363–W367
 66. Kozakov, D., Hall, D. R., Beglov, D., Brenke, R., Comeau, S. R., Shen, Y., Li, K., Zheng, J., Vakili, P., Paschalidis, I. C., and Vajda, S. (2010) Achieving reliability and high accuracy in automated protein docking: ClusPro, PIPER, SOU, and stability analysis in CAPRI rounds 13–19. *Proteins* **78**, 3124–3130
 67. Li, X., Moal, I. H., and Bates, P. A. (2010) Detection and refinement of encounter complexes for protein-protein docking: taking account of macromolecular crowding. *Proteins* **78**, 3189–3196
 68. Andrusier, N., Nussinov, R., and Wolfson, H. J. (2007) FireDock: fast interaction refinement in molecular docking. *Proteins* **69**, 139–159
 69. Mashlach, E., Schneidman-Duhovny, D., Andrusier, N., Nussinov, R., and Wolfson, H. J. (2008) FireDock: a web server for fast interaction refinement in molecular docking. *Nucleic Acids Res.* **36**, W229–W232
 70. Gray, J. J., Moughon, S., Wang, C., Schueler-Furman, O., Kuhlman, B., Rohl, C. A., and Baker, D. (2003) Protein-protein docking with simultaneous optimization of rigid-body displacement and side-chain conformations. *J. Mol. Biol.* **331**, 281–299
 71. Wang, D. F., Wiest, O. G., and Helquist, P. (2005) Homology modeling, docking and molecular dynamics simulation of class IHDACs. *Abstr. Papers Am. Chem. Soc.* **230**, U1360–U1361
 72. Wang, J. G., Xiao, Y. J., Li, Y. H., Ma, Y., and Li, Z. M. (2007) Identification of some novel AHAS inhibitors via molecular docking and virtual screening approach. *Bioorg. Med. Chem.* **15**, 374–380
 73. Clamp, M., Cuff, J., Searle, S. M., and Barton, G. J. (2004) The Jalview Java alignment editor. *Bioinformatics* **20**, 426–427
 74. Dolinsky, T. J., Czodrowski, P., Li, H., Nielsen, J. E., Jensen, J. H., Klebe, G., and Baker, N. A. (2007) PDB2PQR: expanding and upgrading automated preparation of biomolecular structures for molecular simulations. *Nucleic Acids Res.* **35**, W522–W525
 75. Dolinsky, T. J., Nielsen, J. E., McCammon, J. A., and Baker, N. A. (2004) PDB2PQR: an automated pipeline for the setup of Poisson-Boltzmann

- electrostatics calculations. *Nucleic Acids Res.* **32**, W665–W667
76. Callenberg, K. M., Choudhary, O. P., de Forest, G. L., Gohara, D. W., Baker, N. A., and Grabe, M. (2010) APBSmem: a graphical interface for electrostatic calculations at the membrane. *PLoS One* 10.1371/journal.pone.0012722
77. Sitkoff, D., Sharp, K. A., and Honig, B. (1994) Correlating solvation free energies and surface tensions of hydrocarbon solutes. *Biophys. Chem.* **51**, 397–403; discussion 404–399
78. Jo, S., Kim, T., Iyer, V. G., and Im W. (2008) CHARMM-GUI: a Web-based graphical user interface for CHARMM. *J. Comput. Chem.* **29**, 1859–1865
79. Miller, L. J., Chen, Q., Lam, P. C., Pinon, D. I., Sexton, P. M., Abagyan, R., and Dong, M. (2011) Refinement of glucagon-like peptide 1 docking to its intact receptor using mid-region photolabile probes and molecular modeling. *J. Biol. Chem.* **286**, 15895–15907